inegi driving science & innovation

CONVERTING KNOWLEDGE INTO VALUE FOR OVER 35 YEARS

Since 1986

Multi-scale Modelling of Complex Materials undergoing Strain Gradients and Damage

Severo Ochoa Seminar

Igor A. Rodrigues Lopes
ilopes@inegi.up.pt

U.PORTO

BSC-CNS, Barcelona, 21 February 2024

INTRODUCTION

Research experience

Senior researcher at INEGI

2013 – MSc in Mechanical Engineering (FEUP)
- Multi-scale analysis of porous materials

2014-2019 – PhD in Mechanical Engineering (FEUP)
- Second-order computational homogenization (strain-gradients)
- Implementation of FE2 analyses in in-house code
- Parallel computing
- Lagrange multiplier method for more efficient multi-scale analysis

2020-2022 – TREAL - CleanSky2 project (FEUP)
- Finite strain visco-elastic – visco-plastic model for composites
- Finite strain smeared crack model for composites

2022-2026 – DIDEAROT - HORIZON project (INEGI)
- Damage models for composites (micro and meso-scales)
- Surrogate models for composites

Other Interests
- Multi-scale modelling of fracture
- Second-order homogenization for metamaterials and damage

ABOUT INEGI / FEUP / U.Porto

Research and Technology Organisation

Institute of Science and Innovation in Mechanical and Industrial Engineering

inegi driving science & innovation

Founded in 1986

9 267 m2

Facilities - Porto

INNOVATION AND TECHNOLOGY TRANSFER

RESEARCH & DEVELOPMENT

SERVICES

Consulting
Laboratory Services
Advanced Training

- NEW COMPOSITE MATERIALS AND PROCESSES
- METALLOGRAPHY AND ADVANCED CASTING PROCESSES
- METAL FORMING
- ADDITIVE MANUFACTURING
- COMPUTATIONAL MECHANICS
- STRUCTURAL HEALTH MONITORING
- TRIBOLOGY, VIBRATIONS AND DYNAMICS
- MECHANICAL DESIGN
- INSTRUMENTATION, AUTOMATION AND CONTROL
- PRODUCT DEVELOPMENT
- BIOMECHANICS
- WIND ENERGY
- ENERGY EFFICIENCY
- OPERATIONS AND SUPPLY CHAIN MANAGEMENT

Multiscale modelling

Rough contact interfaces

Micromechanical analysis

Polycrystalline alloys

Second-order effects

Coupled analysis

Constitutive modelling of deformation

Ductile metallic materials

Amorphous polymeric materials

Hexagonal compact packed materials

Fibre reinforced polymeric materials

Links

Large Strain Implicit Non-Linear Analysis of Solids Linking Scales

Computational methods

Contact modelling

Incompressible deformation

Non-local ductile damage

High performance computing

CM2S

Computational Multi-Scale Modeling of Solids and Structures

U.PORTO

FEUP FACULDADE DE ENGENHARIA UNIVERSIDADE DO PORTO

COMPUTATIONAL HOMOGENISATION

COMPUTATIONAL HOMOGENISATION
CONCEPT

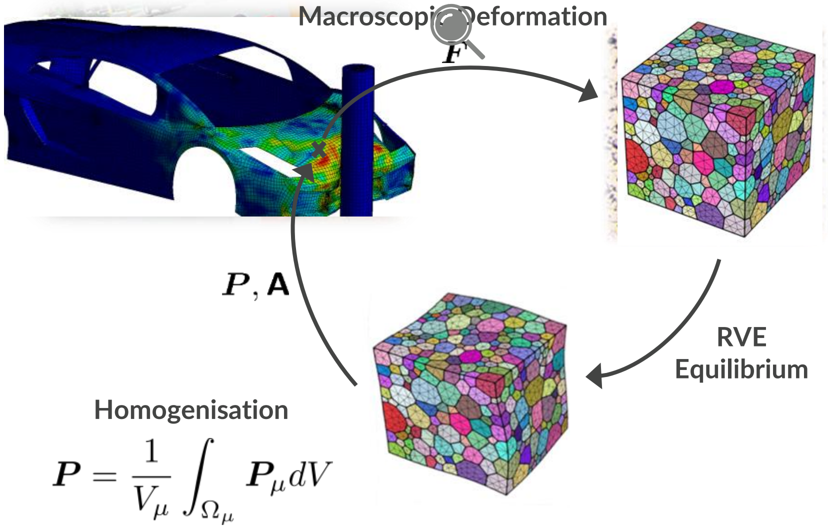

A **computationally efficient solution of the RVE problem** is critical in these applications, since all of them rely on a large number of micro-scale simulations!

A **Representative Volume Element (RVE)** is used to model the microstructure.

Only **constitutive models for individual micro-constituents** are needed. The resulting **compound response is naturally accounted for**.

Suitable for **arbitrary material behaviour** and geometrical **evolution of the microstructure**.

Enables the incorporation of **complex microstructural geometries** together with **large deformations**.

Applications:

- **FE^2 simulations**
- **Parametric studies** (for instance, to generate macroscopic yield surfaces)
- **Topology optimization**
- **Response database** to build **reduced-order models** or to apply in **data-driven frameworks**

COMPUTATIONAL HOMOGENISATION

KINEMATIC CONSTRAINTS

Following the Method of Multi-Scale Virtual Power

[Blanco et al. (2016), *Arch Computat Methods Eng* 23(2) 191-253]

Kinematic insertion

$$\boldsymbol{u}_\mu = (\boldsymbol{F} - \boldsymbol{I})\,\boldsymbol{Y} + \boxed{\tilde{\boldsymbol{u}}}$$

RVE problem unknown

Kinematic homogenization

$$\boldsymbol{F} = \frac{1}{V_\mu}\int_{\Omega_\mu} \boldsymbol{F}_\mu d\Omega_\mu$$

Kinematic admissibility

$$\int_{\Omega_\mu} \nabla_Y \tilde{\boldsymbol{u}} dV = \boldsymbol{0} \Rightarrow \int_{\partial\Omega_\mu} \tilde{\boldsymbol{u}} \otimes \boldsymbol{N} dA = \boldsymbol{0}$$

COMPATIBILITY

Minimal constraint (boundary uniform traction condition)

$$\int_{\partial\Omega_\mu} \tilde{\boldsymbol{u}} \otimes \boldsymbol{N} dA = \boldsymbol{0}$$

Periodic boundary condition

$$\tilde{\boldsymbol{u}}(\boldsymbol{Y}^+) = \tilde{\boldsymbol{u}}(\boldsymbol{Y}^-)$$
$$\boldsymbol{N}(\boldsymbol{Y}^+) = -\boldsymbol{N}(\boldsymbol{Y}^-)$$

Linear boundary condition

$$\tilde{\boldsymbol{u}} = \boldsymbol{0}, \text{ on } \partial\Omega_\mu$$

Spaces of admissible solutions:

$$\tilde{\mathcal{V}}^{linear} \subset \tilde{\mathcal{V}}^{periodic} \subset \tilde{\mathcal{V}}^{u.traction}$$

COMPUTATIONAL HOMOGENISATION

MICRO-SCALE EQUILIBRIUM PROBLEM – CONDENSATION METHOD

Hill-Mandel Principle

$$\boldsymbol{P} : \delta \boldsymbol{F} = \frac{1}{V_\mu} \int_{\Omega_\mu} \boldsymbol{P}_\mu : (\delta \boldsymbol{F} + \nabla_Y \delta \tilde{\boldsymbol{u}})\, dV$$

$$\forall \delta \boldsymbol{F},\ \delta \tilde{\boldsymbol{u}} \in \delta \tilde{\mathcal{V}} \text{ and } \tilde{\boldsymbol{u}} \in \tilde{\mathcal{V}}$$

$\delta \boldsymbol{F} = \mathbf{0}$

Micro-Scale Weak Equilibrium

$$\int_{\Omega_\mu} \boldsymbol{P}_\mu : \nabla_Y \delta \tilde{\boldsymbol{u}} dV = 0, \quad \forall \tilde{\boldsymbol{u}} \in \tilde{\mathcal{V}}$$

Finite Element Solution

$$\mathbf{K} \Delta \tilde{\mathbf{u}} = -\mathbf{r}$$

Linear boundary condition

$$\left[\ \mathbf{k}^{ii}\ \right] \{\Delta \tilde{\mathbf{u}}^i\} = -\{\mathbf{f}^i\}$$

(boundary dofs elimination)

Periodic boundary condition (conform mesh)

$$\left[\begin{array}{c|c} \mathbf{k}^{ii} & \mathbf{k}^{i+} + \mathbf{k}^{i-} \\ \mathbf{k}^{+i} + \mathbf{k}^{-i} & \mathbf{k}^{++} + \mathbf{k}^{-+} + \mathbf{k}^{+-} + \mathbf{k}^{--} \end{array}\right] \begin{Bmatrix} \Delta \tilde{\mathbf{u}}^i \\ \Delta \tilde{\mathbf{u}}^+ \end{Bmatrix} = -\begin{Bmatrix} \mathbf{f}^i \\ \mathbf{f}^+ + \mathbf{f}^- \end{Bmatrix}$$

(boundary dofs standard condensation)

Uniform traction condition

(results in multi-point constraints)

$$\int_{\partial \Omega_\mu} \tilde{\boldsymbol{u}} \otimes \boldsymbol{N} dA = \mathbf{0} \Rightarrow \mathbf{C} \tilde{\mathbf{u}} = \mathbf{0} \qquad \Delta \tilde{\mathbf{u}} = \begin{Bmatrix} \Delta \tilde{\mathbf{u}}^i \\ \Delta \tilde{\mathbf{u}}^f \\ \Delta \tilde{\mathbf{u}}^d \\ \Delta \tilde{\mathbf{u}}^p \end{Bmatrix} \qquad \Delta \tilde{\mathbf{u}}^p = \mathbf{0} \quad \Delta \tilde{\mathbf{u}}^d = \boldsymbol{\alpha} \Delta \tilde{\mathbf{u}}^f$$

$$\boldsymbol{\alpha} = \left[\mathbf{C}^d\right]^{-1} \mathbf{C}^f$$

$$\left[\begin{array}{c|c} \mathbf{k}^{ii} & \mathbf{k}^{if} + \mathbf{k}^{id} \boldsymbol{\alpha} \\ \mathbf{k}^{fi} + \boldsymbol{\alpha}^T \mathbf{k}^{di} & \mathbf{k}^{ff} + \boldsymbol{\alpha}^T \mathbf{k}^{df} + \mathbf{k}^{fd} \boldsymbol{\alpha} + \boldsymbol{\alpha} \mathbf{k}^{dd} \boldsymbol{\alpha}^T \end{array}\right] \begin{Bmatrix} \Delta \tilde{\mathbf{u}}^i \\ \Delta \tilde{\mathbf{u}}^f \end{Bmatrix} = -\begin{Bmatrix} \mathbf{f}^i \\ \mathbf{f}^f + \boldsymbol{\alpha}^T \mathbf{f}^d \end{Bmatrix}$$

MICRO-SCALE EQUILIBRIUM PROBLEM – LAGRANGE MULTIPLIER METHOD

Hill-Mandel Principle

$$\boldsymbol{P} : \delta \boldsymbol{F} = \frac{1}{V_\mu} \left[\int_{\Omega_\mu} \boldsymbol{P}_\mu : (\delta \boldsymbol{F} + \nabla_Y \delta \tilde{\boldsymbol{u}})\, dV - \delta \boldsymbol{L} : \left(\int_{\partial\Omega_\mu} \tilde{\boldsymbol{u}} \otimes \boldsymbol{N} dA \right) - \boldsymbol{L} : \left(\int_{\partial\Omega_\mu} \delta\tilde{\boldsymbol{u}} \otimes \boldsymbol{N} dA \right) \right]$$

$$\forall\, (\delta\boldsymbol{F}, \delta\tilde{\boldsymbol{u}}, \delta\boldsymbol{L})$$

$$\delta \boldsymbol{F} = \boldsymbol{0}$$

Micro-Scale Weak Equilibrium

$$\int_{\Omega_\mu} \boldsymbol{P}_\mu : \nabla_Y \delta \tilde{\boldsymbol{u}} dV - \delta \boldsymbol{L} : \left(\int_{\partial\Omega_\mu} \tilde{\boldsymbol{u}} \otimes \boldsymbol{N} dA \right) - \boldsymbol{L} : \left(\int_{\partial\Omega_\mu} \delta\tilde{\boldsymbol{u}} \otimes \boldsymbol{N} dA \right) = 0$$

Finite Element Solution

$$\begin{bmatrix} \mathbf{k}^{ii} & \mathbf{k}^{if} & \mathbf{0} \\ \mathbf{k}^{fi} & \mathbf{k}^{ff} & \mathbf{C}_L^T \\ \mathbf{0} & \mathbf{C}_L & \mathbf{0} \end{bmatrix} \begin{Bmatrix} \Delta\tilde{\mathbf{u}}^i \\ \Delta\tilde{\mathbf{u}}^f \\ \Delta\boldsymbol{\lambda}_L \end{Bmatrix} = - \begin{Bmatrix} \mathbf{f}^i \\ \mathbf{f}^f - \mathbf{C}_L^T \boldsymbol{\lambda}_L \\ \mathbf{C}_L \tilde{\mathbf{u}}^f \end{Bmatrix}$$

Homogenised Stress

$$\boldsymbol{P} = \frac{1}{V_\mu} \int_{\Omega_\mu} \boldsymbol{P}_\mu dV = \boldsymbol{L}$$

Macroscopic consistent tangent

$$\mathbf{A} = \frac{\partial \mathbf{P}}{\partial \mathbf{F}} = \boxed{\frac{\partial \boldsymbol{\lambda}_L}{\partial \mathbf{F}}}$$

$$\begin{bmatrix} \mathbf{k}^{ii} & \mathbf{k}^{if} & \mathbf{0} \\ \mathbf{k}^{fi} & \mathbf{k}^{ff} & \mathbf{C}_L^T \\ \mathbf{0} & \mathbf{C}_L & \mathbf{0} \end{bmatrix} \begin{bmatrix} \dfrac{\partial \tilde{\mathbf{u}}^i}{\partial \mathbf{F}} \\ \dfrac{\partial \tilde{\mathbf{u}}^f}{\partial \mathbf{F}} \\ \boxed{\dfrac{\partial \boldsymbol{\lambda}_L}{\partial \mathbf{F}}} \end{bmatrix} = - \begin{bmatrix} \mathbf{k}^{ii} & \mathbf{k}^{if} & \mathbf{k}^{ip} \\ \mathbf{k}^{fi} & \mathbf{k}^{ff} & \mathbf{k}^{fp} \\ \mathbf{0} & \mathbf{0} & \mathbf{0} \end{bmatrix} \begin{bmatrix} \mathbf{D}^i & \mathbf{D}^f & \mathbf{D}^p \end{bmatrix}$$

I. A. Rodrigues Lopes, B. P. Ferreira, and F. M. Andrade Pires (2021), *Comput. Methods Appl. Mech. Eng.*, vol. 384, p. 113930

COMPUTATIONAL HOMOGENISATION

MORTAR PERIODIC BOUNDARY CONDITION

I. A. Rodrigues Lopes, B. P. Ferreira, and F. M. Andrade Pires (2021), *Comput. Methods Appl. Mech. Eng.*, vol. 384, p. 113930

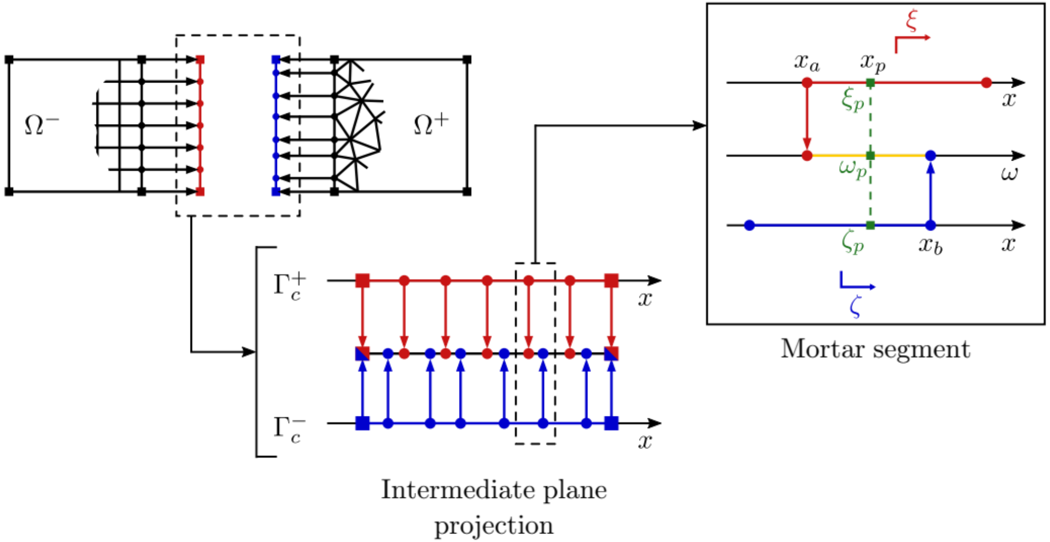

Micro-Scale Weak Equilibrium

$$\int_{\Omega_\mu} \boldsymbol{P}_\mu : \nabla_Y \delta\tilde{\boldsymbol{u}} dV + \int_{\partial\Omega_\mu^+} \delta\boldsymbol{\lambda} \cdot \left(\tilde{\boldsymbol{u}}^+ - \tilde{\boldsymbol{u}}^-\right) dA + \int_{\partial\Omega_\mu^+} \boldsymbol{\lambda} \cdot \left(\delta\tilde{\boldsymbol{u}}^+ - \delta\tilde{\boldsymbol{u}}^-\right) dA = 0$$

Finite Element Solution

$$\begin{bmatrix} \mathbf{k}^{ii} & \mathbf{k}^{i-} & \mathbf{k}^{i+} & \mathbf{0} \\ \mathbf{k}^{-i} & \mathbf{k}^{--} & \mathbf{k}^{-+} & -[\mathbf{A}^m]^T \\ \mathbf{k}^{+i} & \mathbf{k}^{+-} & \mathbf{k}^{++} & \mathbf{D}^{nm} \\ \mathbf{0} & -\mathbf{A}^m & \mathbf{D}^{nm} & \mathbf{0} \end{bmatrix} \begin{Bmatrix} \Delta\tilde{\mathbf{u}}^i \\ \Delta\tilde{\mathbf{u}}^- \\ \Delta\tilde{\mathbf{u}}^+ \\ \Delta\boldsymbol{\lambda} \end{Bmatrix} = - \begin{Bmatrix} \mathbf{f}^i \\ \mathbf{f}^- - [\mathbf{A}^m]^T \boldsymbol{\lambda} \\ \mathbf{f}^+ + \mathbf{D}^{nm}\boldsymbol{\lambda} \\ \mathbf{D}^{nm}\tilde{\mathbf{u}}^+ - \mathbf{A}^m\tilde{\mathbf{u}}^- \end{Bmatrix}$$

COMPUTATIONAL HOMOGENISATION

EFFICIENCY OF THE LAGRANGE MULTIPLIER APPROACH

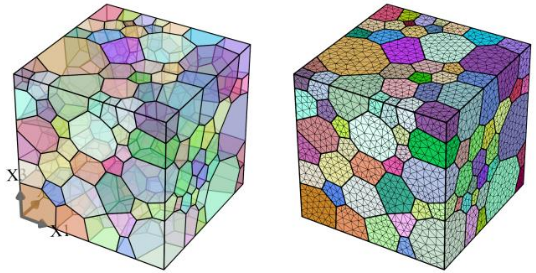

250 grains

62248 tetra 4 elements

11908 nodes

Anisotropic Saint Venant-Kirchhoff hyperelasticity:

$D_{11} = 168.4$ GPa, $D_{12} = 121.4$ GPa, and $D_{44} = 75.4$ GPa

$$\mathbf{D}^e = \begin{bmatrix} D_{11} & D_{12} & D_{12} & 0 & 0 & 0 \\ & D_{11} & D_{12} & 0 & 0 & 0 \\ & & D_{11} & 0 & 0 & 0 \\ & & & D_{44} & 0 & 0 \\ & sym. & & & D_{44} & 0 \\ & & & & & D_{44} \end{bmatrix}$$

$$\boldsymbol{F} = \begin{bmatrix} 1.0 & 0.5 & 0.0 \\ 0.0 & 1.2 & 0.0 \\ 0.0 & 0.0 & 1.0 \end{bmatrix}$$

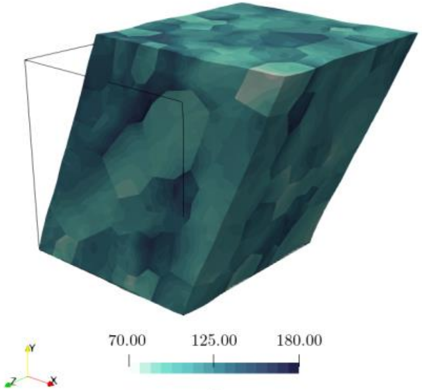

		Time (s)		
		Cond.	L.M.	**Speedup**
Uniform traction	solver	140.44	3.45	40.71
	iteration	146.90	3.96	37.10
	total	7647	232	32.90
Mortar periodic	solver	10.67	13.03	0.82
	iteration	99.79	13.29	7.51
	total	4812	669	7.19

	Mem. peak (MB)		**Savings (%)**
	Cond.	L.M.	
Uniform traction	9492	761	**92.0**
Mortar periodic	6046	1238	**79.5**

I. A. Rodrigues Lopes, B. P. Ferreira, and F. M. Andrade Pires (2021), *Comput. Methods Appl. Mech. Eng.*, vol. 384, p. 113930

COMPUTATIONAL HOMOGENISATION

EFFICIENCY OF THE LAGRANGE MULTIPLIER APPROACH

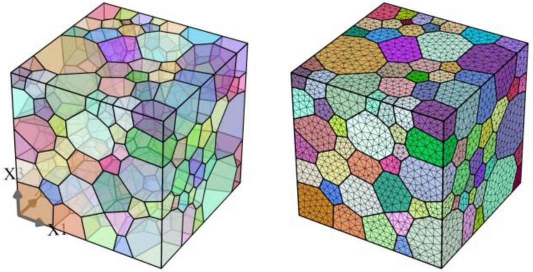

	Sparsity (%)	
	Cond.	L.M.
Uniform traction	7.8075	0.7037
Mortar periodic	0.9994	0.5526

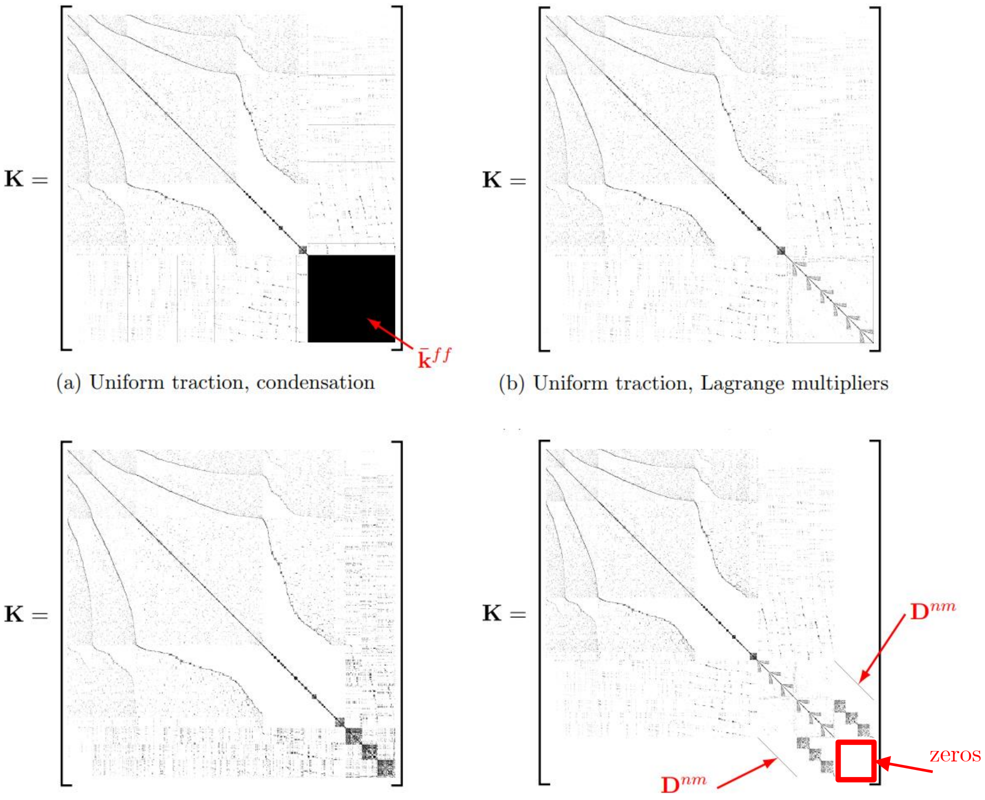

(a) Uniform traction, condensation

(b) Uniform traction, Lagrange multipliers

(c) Mortar periodic, condensation

(d) Mortar periodic, Lagrange multipliers

I. A. Rodrigues Lopes, B. P. Ferreira, and F. M. Andrade Pires (2021), *Comput. Methods Appl. Mech. Eng.*, vol. 384, p. 113930

COMPUTATIONAL HOMOGENISATION

EFFICIENCY OF THE LAGRANGE MULTIPLIER APPROACH

200 elements with 4 Gauss points: 800 RVE simulations in each macro-iteration
Parallelization with 16 CPUs [Rodrigues Lopes et al. (2018) Comp.Mech. 61 (1-2) 157-180]

	Matrix	Inclusions
Young modulus (E) [GPa]	2.0	74.0
Poisson ratio (ν)	0.4	0.2

RVE

896 quad8 elements

2793 nodes

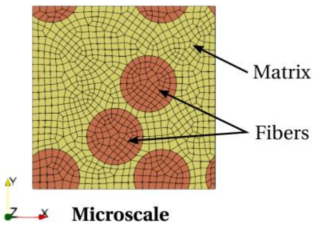

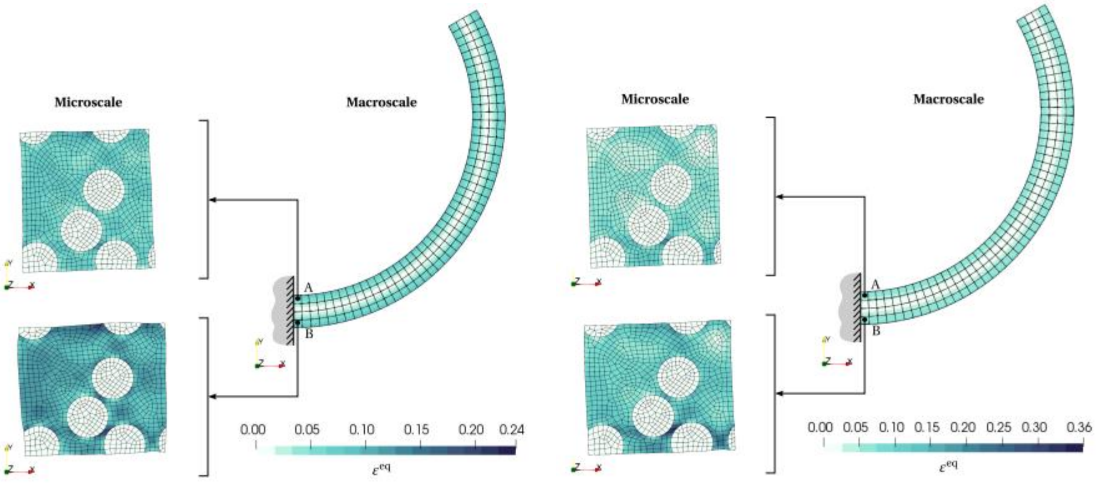

(a) Uniform traction (b) Mortar periodic

		Time (s) Cond.	Time (s) L.M.	**Speedup**
Uniform traction	solver	0.097	0.067	1.45
	iteration	0.132	0.089	1.48
	total	5.54	3.74	1.48
Mortar periodic	solver	0.063	0.083	0.76
	iteration	0.126	0.104	1.21
	total	5.16	4.20	1.22

		Time (s) Cond.	Time (s) L.M.	**Speedup**
Uniform Traction	iteration	37.3	15.3	**2.44**
	total	5039	2007	**2.51**
Periodic Mortar	iteration	31.5	17.1	**1.84**
	total	4371	2280	**1.92**

I. A. Rodrigues Lopes, B. P. Ferreira, and F. M. Andrade Pires (2021), *Comput. Methods Appl. Mech. Eng.*, vol. 384, p. 113930

PARALLEL COMPUTING

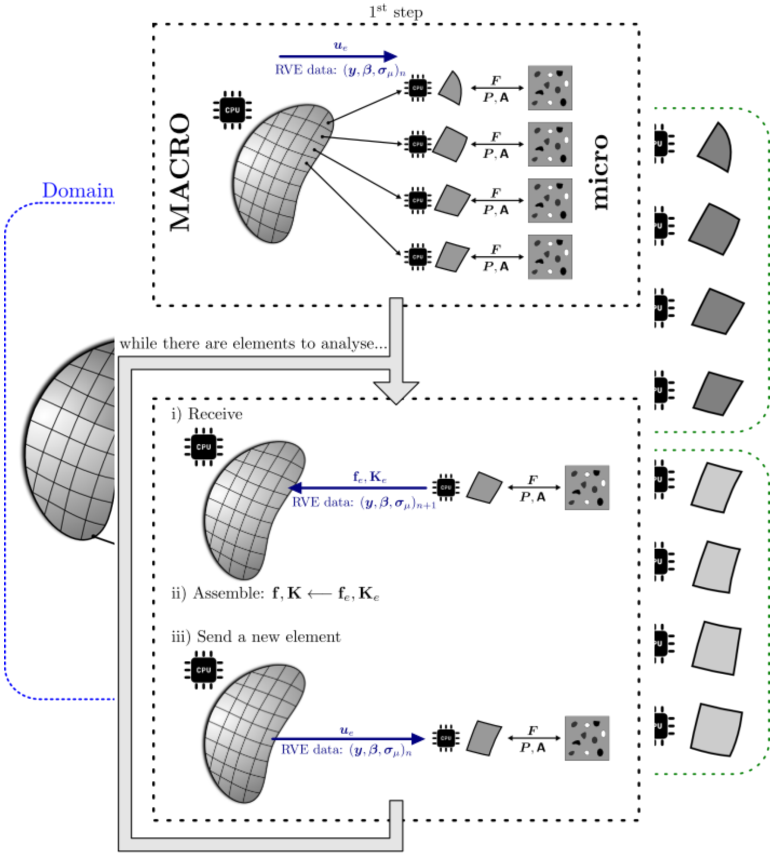

Atlanticus
BEOWULF CLUSTER

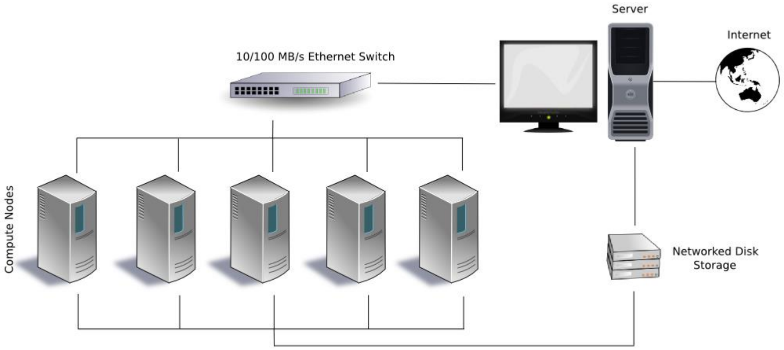

[Rodrigues Lopes et al. (2018) Comp.Mech. 61 (1-2) 157-180]

COMPUTATIONAL HOMOGENISATION

PARALLEL COMPUTING

MACRO

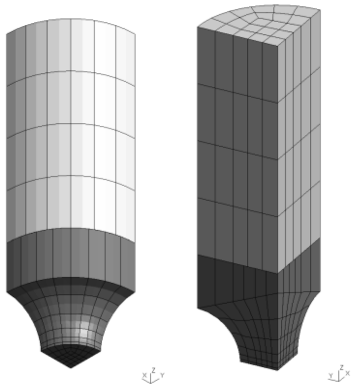

84 Hexa20 light grey elements

224 Hexa20 dark grey elements

MICRO

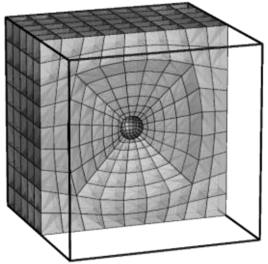

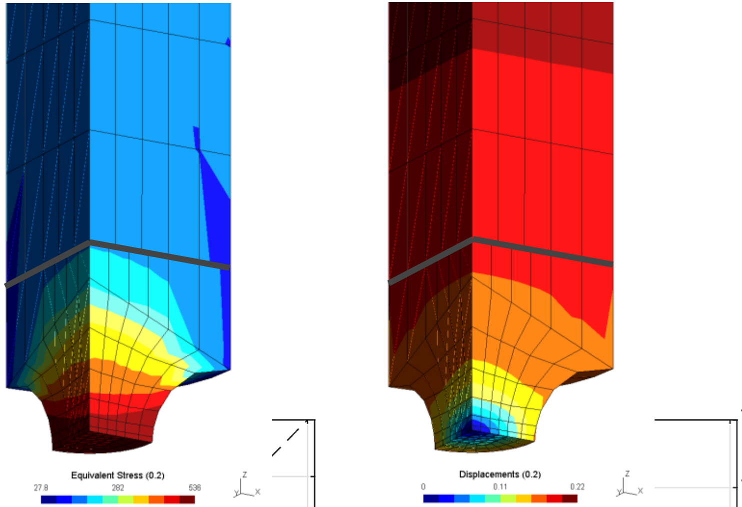

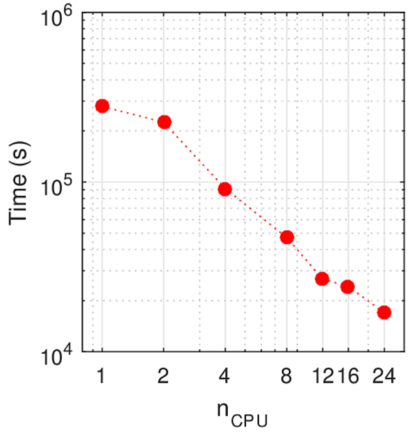

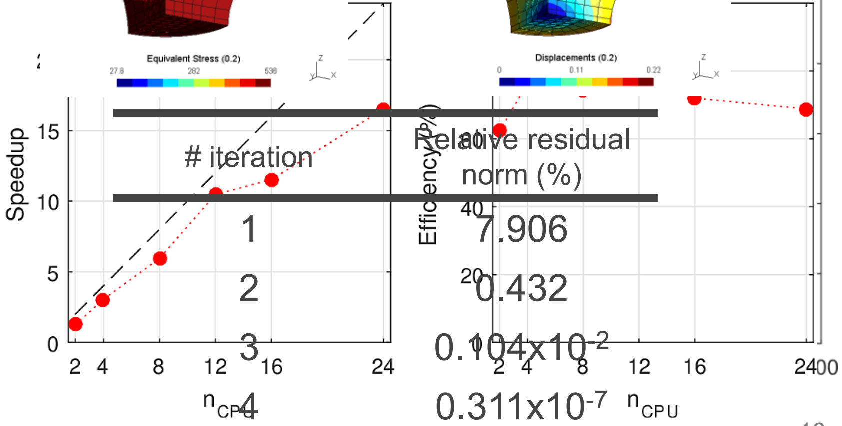

# iteration	Relative residual norm (%)
1	7.906
2	0.432
3	0.104×10^{-2}
4	0.311×10^{-7}

[Rodrigues Lopes et al. (2018) Comp.Mech. 61 (1-2) 157-180]

COMPUTATIONAL HOMOGENISATION
PARALLEL COMPUTING

[Rui Coelho (2021), Internal Report]

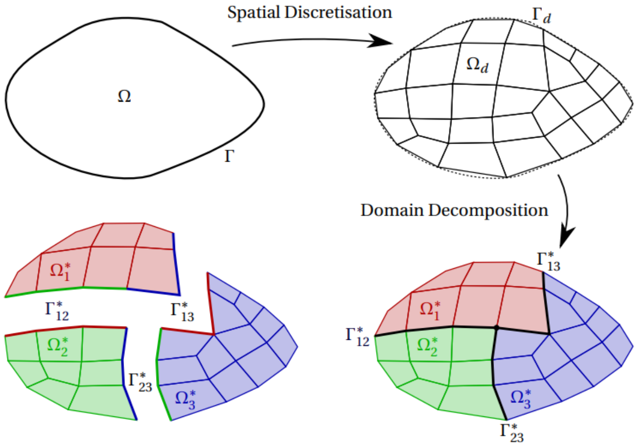

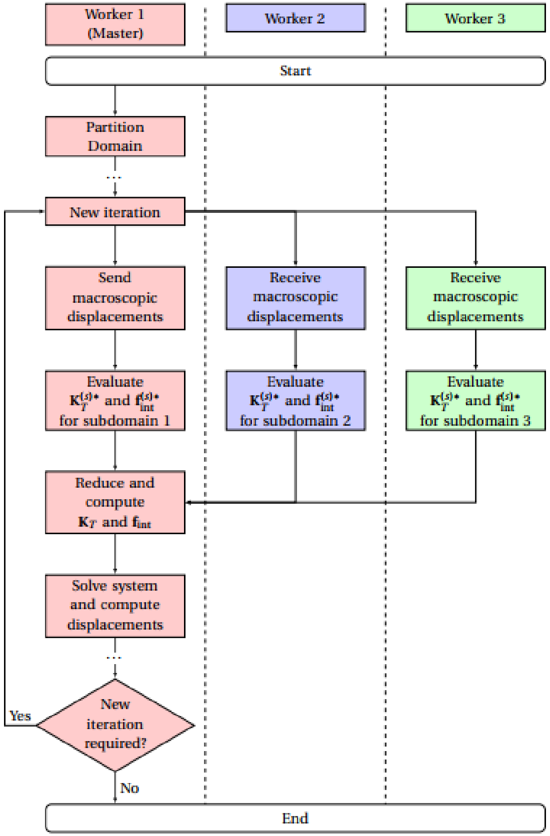

COMPUTATIONAL HOMOGENISATION WITH STRAIN GRADIENTS

SECOND-ORDER COMPUTATIONAL HOMOGENISATION

CONCEPT

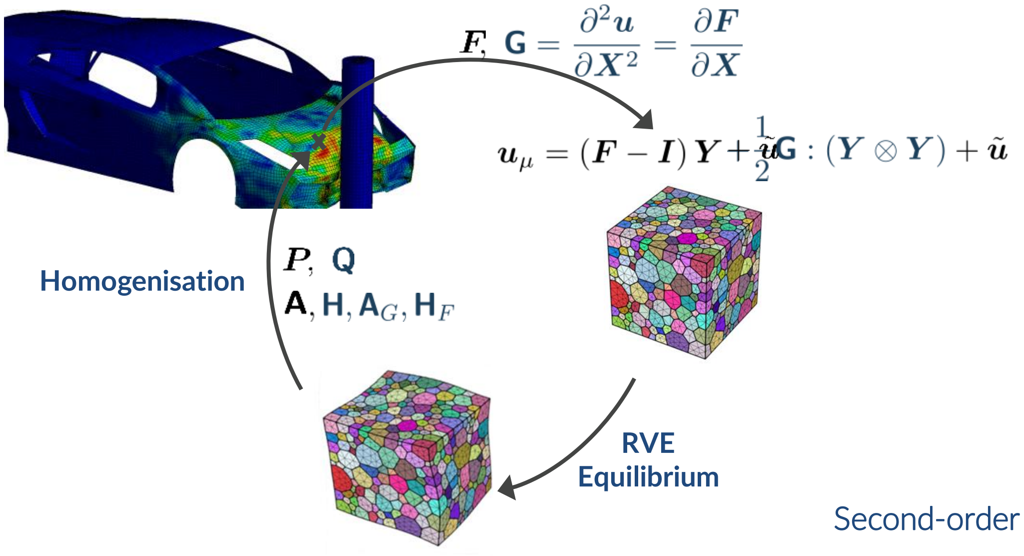

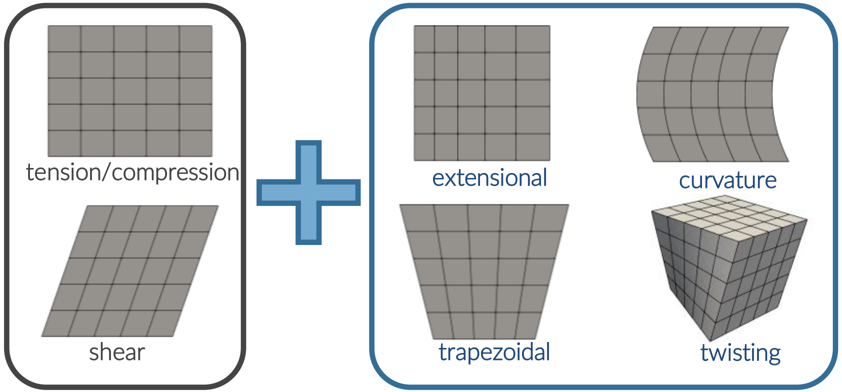

Second-order homogenisation:

- **Second-gradient continuum** at the macro-scale
- Linear variation of the macro-deformation gradient
- **Second-order deformation modes** at the RVE
- The RVE length results in a length scale parameter
- Captures **size effects**

SECOND-ORDER COMPUTATIONAL HOMOGENISATION

POTENTIAL APPLICATIONS

Interesting applications for second-order homogenisation:

- Analysis and design of structures subjected to **deformations with high curvatures**
- Metal sheet forming
- Design of actuators based on **phase transformation**
- Deformation of **woven composites**
- Modelling the behaviour **meta-materials**

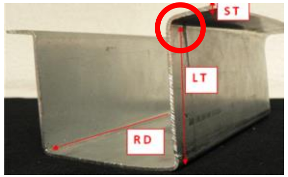

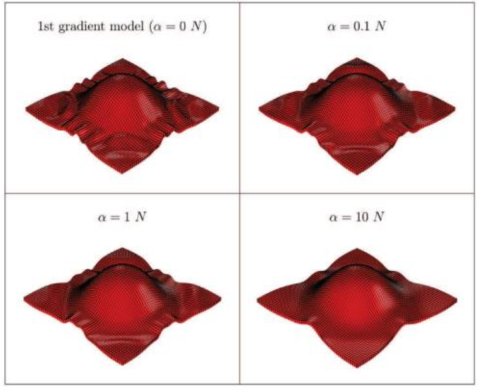

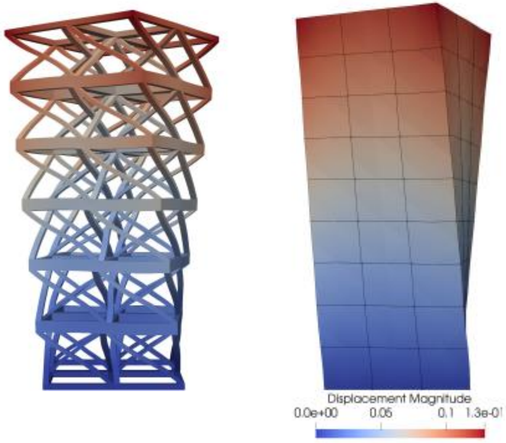

SECOND-ORDER COMPUTATIONAL HOMOGENISATION

FORMULATION

Formulation detailed in: Rodrigues Lopes, I. A., & Andrade Pires, F. M. (2022). *Comput. Methods in Appl. Mech. Engrg*, *392*, 114714.

Review in: Rodrigues Lopes, I. A., & Andrade Pires, F. M. (2022). *Arch. Comput. Methods Eng.*, 29(3), pp. 1339–1393

Macro 2nd gradient continuum

$\boldsymbol{F}, \mathbf{G}$

Micro 1st gradient continuum

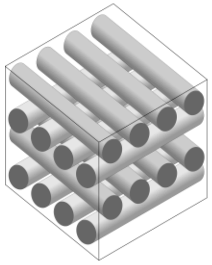

POSTULATED

Kinematic insertion

$$\boldsymbol{u}_\mu = (\boldsymbol{F} - \boldsymbol{I})\,\boldsymbol{Y} + \frac{1}{2}\mathbf{G} : (\boldsymbol{Y} \otimes \boldsymbol{Y}) + \tilde{\boldsymbol{u}}$$

Kinematic homogenisation

$$\boldsymbol{F} = \frac{1}{V_\mu}\int_{\Omega_\mu} \boldsymbol{F}_\mu d\Omega_\mu$$

$$\mathbf{G} = \frac{1}{V_\mu}\int_{\Omega_\mu} (\nabla_Y \boldsymbol{u}_\mu \otimes \boldsymbol{Y}) \cdot \boldsymbol{J}^{-1} d\Omega_\mu$$

Kinematic admissibility

1st Constraint: $\displaystyle\int_{\Omega_\mu} \nabla_Y \tilde{\boldsymbol{u}} dV = \mathbf{0} \Rightarrow \int_{\partial\Omega_\mu} \tilde{\boldsymbol{u}} \otimes \boldsymbol{N} dA = \mathbf{0}$

2nd Constraint: $\displaystyle\int_{\Omega_\mu} (\nabla_Y \tilde{\boldsymbol{u}} \otimes \boldsymbol{Y}) \cdot \boldsymbol{J}^{-1} dV = \mathbf{0}$

COMPATIBILITY

SECOND-ORDER COMPUTATIONAL HOMOGENISATION

MICRO-SCALE EQUILIBRIUM PROBLEM – LAGRANGE MULTIPLIERS

Principle of Multi-Scale Virtual Power

$$
\begin{aligned}
\underbrace{\boldsymbol{P} : \delta\boldsymbol{F} + \mathbf{Q} \vdots \delta\mathbf{G}}_{\text{Macro}} = \frac{1}{V_\mu} \Bigg[\int_{\Omega_\mu} & \boldsymbol{P}_\mu : (\delta\boldsymbol{F} + \delta\mathbf{G} \cdot \boldsymbol{Y} + \nabla_Y \delta\tilde{\boldsymbol{u}})\, dV \\
& - \delta\boldsymbol{L} : \left(\int_{\partial\Omega_\mu} \tilde{\boldsymbol{u}} \otimes \boldsymbol{N} dA \right) - \boldsymbol{L} : \left(\int_{\partial\Omega_\mu} \delta\tilde{\boldsymbol{u}} \otimes \boldsymbol{N} dA \right) \\
& - \delta\mathbf{M} \vdots \left(\int_{\Omega_\mu} (\nabla_Y \tilde{\boldsymbol{u}} \otimes \boldsymbol{Y}) \cdot \boldsymbol{J}^{-1} dV \right) \\
& - \mathbf{M} \vdots \left(\int_{\Omega_\mu} (\nabla_Y \delta\tilde{\boldsymbol{u}} \otimes \boldsymbol{Y}) \cdot \boldsymbol{J}^{-1} dV \right) \Bigg], \quad \forall\, (\delta\boldsymbol{F}, \delta\mathbf{G}, \delta\tilde{\boldsymbol{u}}, \delta\boldsymbol{L}, \delta\mathbf{M}) \,.
\end{aligned}
$$

Micro-Scale Weak Equilibrium: $\delta\boldsymbol{F} = 0, \;\; \delta\mathbf{G} = 0$

$$
\begin{aligned}
\int_{\Omega_\mu} \boldsymbol{P}_\mu : \nabla_Y \delta\tilde{\boldsymbol{u}} dV - \delta\boldsymbol{L} : & \left(\int_{\partial\Omega_\mu} \tilde{\boldsymbol{u}} \otimes \boldsymbol{N} dA \right) \\
& - \boldsymbol{L} : \left(\int_{\partial\Omega_\mu} \delta\tilde{\boldsymbol{u}} \otimes \boldsymbol{N} dA \right) \\
& - \delta\mathbf{M} \vdots \left(\int_{\Omega_\mu} (\nabla_Y \tilde{\boldsymbol{u}} \otimes \boldsymbol{Y}) \cdot \boldsymbol{J}^{-1} dV \right) \\
& - \mathbf{M} \vdots \left(\int_{\Omega_\mu} (\nabla_Y \delta\tilde{\boldsymbol{u}} \otimes \boldsymbol{Y}) \cdot \boldsymbol{J}^{-1} dV \right) = 0
\end{aligned}
$$

FEM discretisation and linearisation

$$
\left[\begin{array}{c:c:c:c}
\mathbf{K}^{ii} & \mathbf{K}^{ib} & -\mathbf{C}_M^{i,T} & \mathbf{0} \\
\mathbf{K}^{bi} & \mathbf{K}^{bb} & -\mathbf{C}_M^{b,T} & -\mathbf{C}_L^T \\
\mathbf{C}_M^i & \mathbf{C}_M^b & \mathbf{0} & \mathbf{0} \\
\mathbf{0} & \mathbf{C}_L & \mathbf{0} & \mathbf{0}
\end{array} \right]
\left\{ \begin{array}{c}
\Delta\tilde{\mathbf{u}}^i \\
\Delta\tilde{\mathbf{u}}^b \\
\Delta\boldsymbol{\lambda}_M \\
\Delta\boldsymbol{\lambda}_L
\end{array} \right\}
= -
\left\{ \begin{array}{c}
\mathbf{f}^i - \mathbf{C}_M^{i,T} \boldsymbol{\lambda}_M \\
\mathbf{f}^b - \mathbf{C}_M^{b,T} \boldsymbol{\lambda}_M - \mathbf{C}_L^T \boldsymbol{\lambda}_L \\
\mathbf{C}_M \tilde{\mathbf{u}} \\
\mathbf{C}_L \tilde{\mathbf{u}}^b
\end{array} \right\}
$$

Lagrange multiplier method is used to enforce the micro-scale kinematical constraints:

$\boldsymbol{L}$ enforces 1st constraint: $\displaystyle\int_{\partial\Omega_\mu} \tilde{\boldsymbol{u}} \otimes \boldsymbol{N} dA = \mathbf{0}$

$\mathbf{M}$ enforces 2nd constraint: $\displaystyle\int_{\Omega_\mu} (\nabla_Y \tilde{\boldsymbol{u}} \otimes \boldsymbol{Y}) \cdot \boldsymbol{J}^{-1} dV = \mathbf{0}$

MACRO-SCALE CONSISTENT TANGENTS

The macroscopic consistent tangents are needed in a FE^2 framework

$$\frac{\partial \mathbf{r}}{\partial \mathbf{F}} = \mathbf{0} \Rightarrow \begin{bmatrix} \boxed{\frac{\partial \mathbf{f}}{\partial \mathbf{F}}} - \mathbf{C}^T \boxed{\frac{\partial \boldsymbol{\lambda}}{\partial \mathbf{F}}} \\ \mathbf{C} \boxed{\frac{\partial \tilde{\mathbf{u}}}{\partial \mathbf{F}}} \end{bmatrix} = \mathbf{0}$$

$$\boxed{\frac{\partial \mathbf{f}}{\partial \mathbf{F}}} = \frac{\partial \mathbf{f}}{\partial \mathbf{u}} \frac{\partial \mathbf{u}}{\partial \mathbf{F}} = \mathbf{K}\left(\mathbf{D}^T + \boxed{\frac{\partial \tilde{\mathbf{u}}}{\partial \mathbf{F}}}\right)$$

$$\boldsymbol{u}_\mu = (\boldsymbol{F} - \boldsymbol{I}) \cdot \boldsymbol{Y} + \frac{1}{2}\mathbf{G} : (\boldsymbol{Y} \otimes \boldsymbol{Y}) + \tilde{\boldsymbol{u}}$$

$$\Downarrow$$

$$\mathbf{u}_\mu = \mathbf{D}^T (\mathbf{F} - \{\mathbf{I}\}) + \mathbf{V}^T \mathbf{G} + \tilde{\mathbf{u}}$$

(insertion discretisation)

$$\frac{\partial \mathbf{r}}{\partial \mathbf{G}} = \mathbf{0} \Rightarrow \begin{bmatrix} \boxed{\frac{\partial \mathbf{f}}{\partial \mathbf{G}}} - \mathbf{C}^T \boxed{\frac{\partial \boldsymbol{\lambda}}{\partial \mathbf{G}}} \\ \mathbf{C} \boxed{\frac{\partial \tilde{\mathbf{u}}}{\partial \mathbf{G}}} \end{bmatrix} = \mathbf{0}$$

$$\boxed{\frac{\partial \mathbf{f}}{\partial \mathbf{G}}} = \frac{\partial \mathbf{f}}{\partial \mathbf{u}} \frac{\partial \mathbf{u}}{\partial \mathbf{G}} = \mathbf{K}\left(\mathbf{V}^T + \boxed{\frac{\partial \tilde{\mathbf{u}}}{\partial \mathbf{G}}}\right)$$

$$\begin{bmatrix} \mathbf{K} & -\mathbf{C}^T \\ \mathbf{C} & \mathbf{0} \end{bmatrix} \begin{bmatrix} \frac{\partial \tilde{\mathbf{u}}}{\partial \mathbf{F}} & \frac{\partial \tilde{\mathbf{u}}}{\partial \mathbf{G}} \\ \frac{\partial \boldsymbol{\lambda}}{\partial \mathbf{F}} & \frac{\partial \boldsymbol{\lambda}}{\partial \mathbf{G}} \end{bmatrix} = - \begin{bmatrix} \mathbf{K}\mathbf{D}^T & \mathbf{K}\mathbf{V}^T \\ \mathbf{0} & \mathbf{0} \end{bmatrix}$$

$$\mathbb{A} = \frac{\partial \mathbf{P}}{\partial \mathbf{F}} = \frac{\partial \boldsymbol{\lambda}_L}{\partial \mathbf{F}} \qquad \mathbb{A}_G = \frac{\partial \mathbf{P}}{\partial \mathbf{G}} = \frac{\partial \boldsymbol{\lambda}_L}{\partial \mathbf{G}}$$

$$\mathbb{H}_F = \frac{\partial \mathbf{Q}}{\partial \mathbf{F}} = \frac{\partial \boldsymbol{\lambda}_{M^S}}{\partial \mathbf{F}} \qquad \mathbb{H} = \frac{\partial \mathbf{Q}}{\partial \mathbf{G}} = \frac{\partial \boldsymbol{\lambda}_{M^S}}{\partial \mathbf{G}}$$

NUMERICAL EXAMPLE – SIZE EFFECTS IN A BOUNDARY SHEAR LAYER

FE^2 3D boundary shear layer simulation

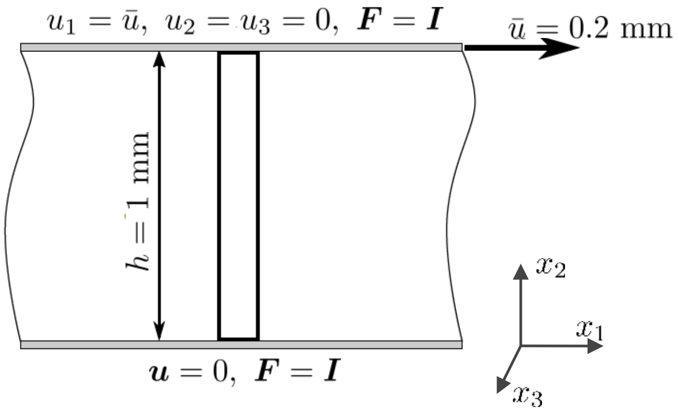

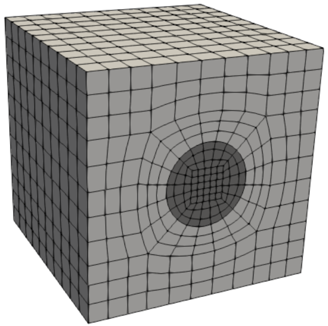

Matrix	Fibre
$E_m = 70$ GPa	$E_f = 700$ GPa
$\nu_m = 0.3$	$\nu_f = 0.3$

2410 Hexa20 elements

8 Gauss points

11088 nodes

The macro-scale second-gradient continuum must be discretized with elements that guarantee C^1 continuity:

- Mixed Finite Elements

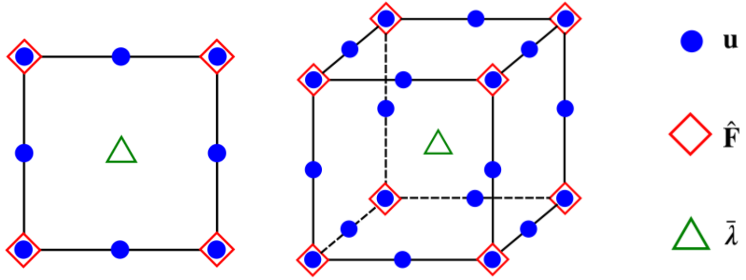

Q8F4L1 H20F8L1

$$\int_{\Omega}\left(\boldsymbol{P} : \delta\boldsymbol{F} + \mathbf{Q} \vdots \nabla_0^s \delta\hat{\boldsymbol{F}} - \delta\left[\boldsymbol{\lambda} : \left(\boldsymbol{F} - \hat{\boldsymbol{F}}\right)\right]\right) dV = \int_{\partial\Omega} \boldsymbol{t}_0 \cdot \delta\boldsymbol{u}\, dA + \int_{\partial\Omega} \boldsymbol{R}_0 : \delta\hat{\boldsymbol{F}}\, dA$$

$$\begin{bmatrix} \mathbf{K}^{uu} & \mathbf{K}^{uF} & \mathbf{K}^{u\lambda} \\ \mathbf{K}^{Fu} & \mathbf{K}^{FF} & \mathbf{K}^{F\lambda} \\ \mathbf{K}^{\lambda u} & \mathbf{K}^{\lambda F} & \mathbf{K}^{\lambda\lambda} \end{bmatrix}^{(k)} \begin{Bmatrix} \Delta\mathbf{u} \\ \Delta\hat{\mathbf{F}} \\ \Delta\boldsymbol{\lambda} \end{Bmatrix}^{(k+1)} = -\begin{Bmatrix} \mathbf{r}^{u} \\ \mathbf{r}^{F} \\ \mathbf{r}^{\lambda} \end{Bmatrix}^{(k)}$$

SECOND-ORDER COMPUTATIONAL HOMOGENISATION

NUMERICAL EXAMPLE – SIZE EFFECTS IN A BOUNDARY SHEAR LAYER

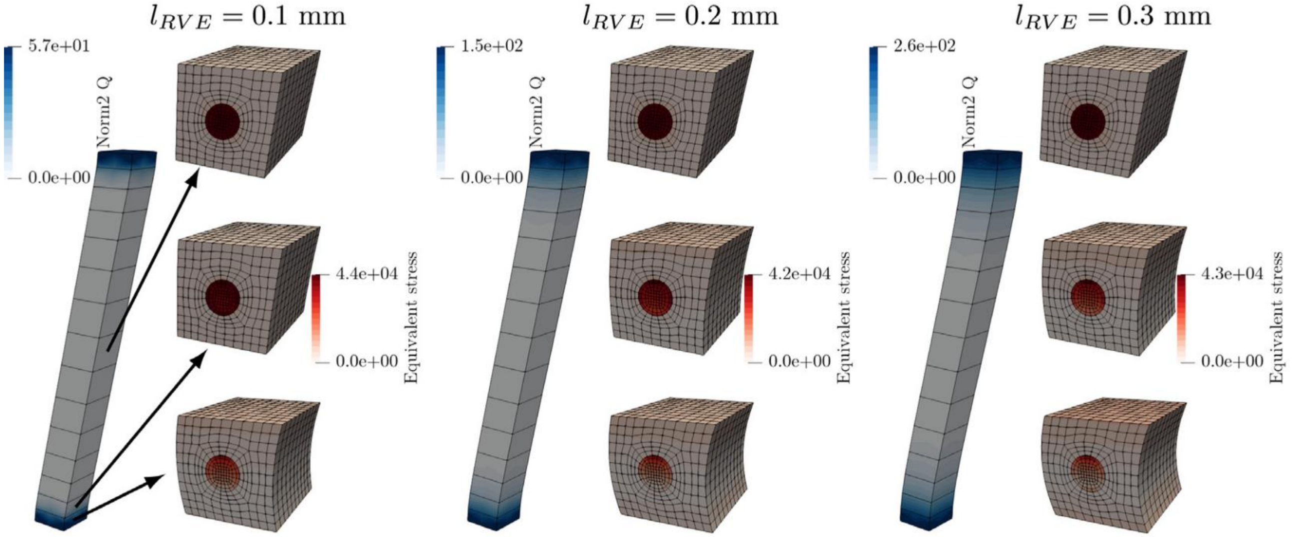

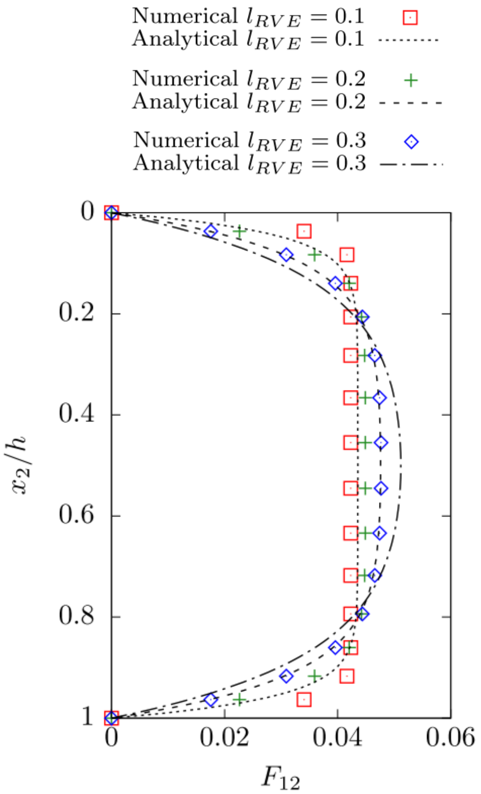

SECOND-ORDER COMPUTATIONAL HOMOGENISATION

NUMERICAL EXAMPLE – POLYCRYSTALLINE MATERIALS

M. Vieira de Carvalho, R. P. Cardoso Coelho, and F. M. A. Pires (2022), *Int. J. Numer. Methods Eng.*, 23, 21, 5155–5200
I. A. Rodrigues Lopes, et al (2023), *Eur. J. Mech. - A/Solids*, 102, 105104.

$l_{RVE} = 0.2$ mm
65 grains

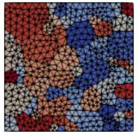

$l_{RVE} = 0.4$ mm
250 grains

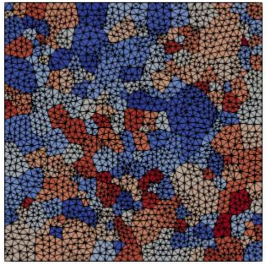

$l_{RVE} = 0.8$ mm
1000 grains

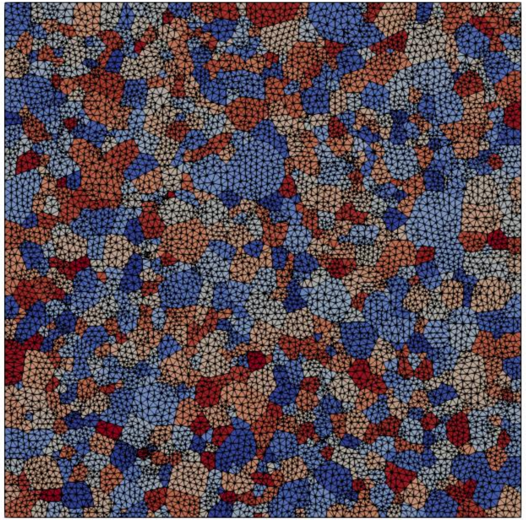

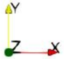

5 realizations for each RVE type

Sandvik Nanoflex

Austenitic stainless steel

C_{11}	282.69	[GPa]
C_{12}	121.15	[GPa]
C_{44}	80.769	[GPa]
ϵ^{pa}	0.01	-
ϵ_0^{pa}	10	-
n_{visco}	8	-
m_{depth}	4	-
$\tilde{\tau}_y$	0.088	[GPa]
K	0.195	[GPa]
γ_0	0.01	-
m	0.6	-

Nadai-Ludwik power-law:

$$\tau_y(\gamma) = \tilde{\tau}_y + K\left(\gamma_0 + \gamma\right)^m$$

SECOND-ORDER COMPUTATIONAL HOMOGENISATION

NUMERICAL EXAMPLE – POLYCRYSTALLINE MATERIALS

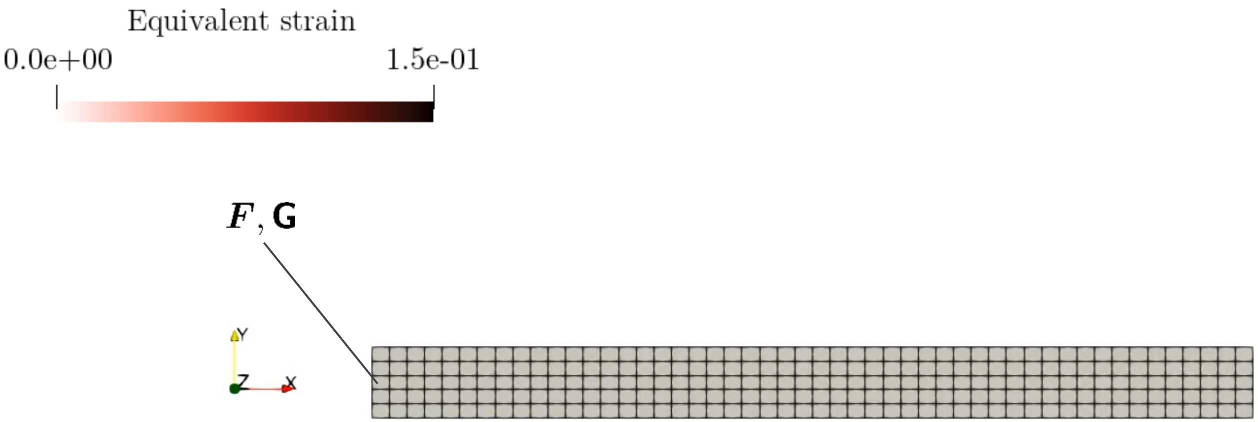

I. A. Rodrigues Lopes, et al (2023), *Eur. J. Mech. - A/Solids*, 102, 105104.

SECOND-ORDER COMPUTATIONAL HOMOGENISATION

NUMERICAL EXAMPLE – POLYCRYSTALLINE MATERIALS

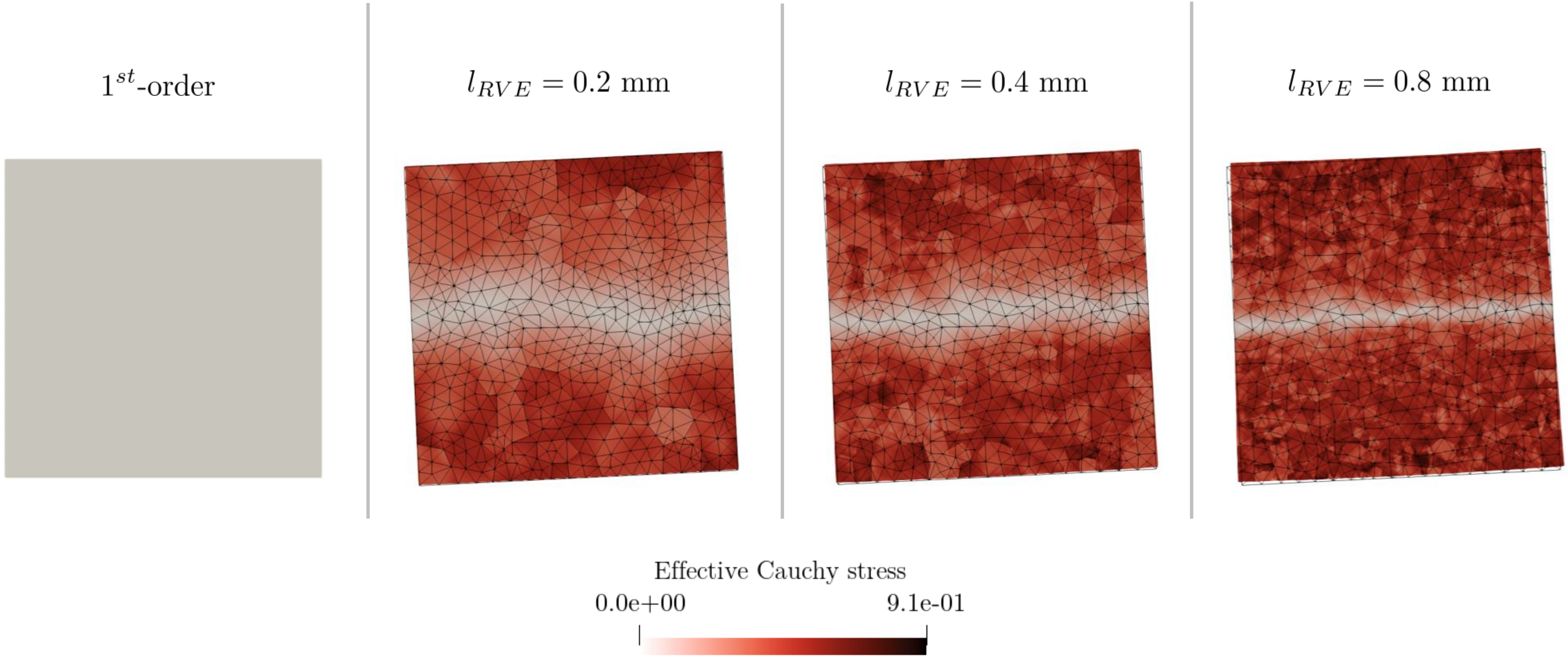

I. A. Rodrigues Lopes, et al (2023), *Eur. J. Mech. - A/Solids*, 102, 105104.

SECOND-ORDER COMPUTATIONAL HOMOGENISATION

NUMERICAL EXAMPLE – MARTENSITIC TRANSFORMATION

$l_{RVE} = 0.8$ mm

1^{st}-order 2^{nd}-order

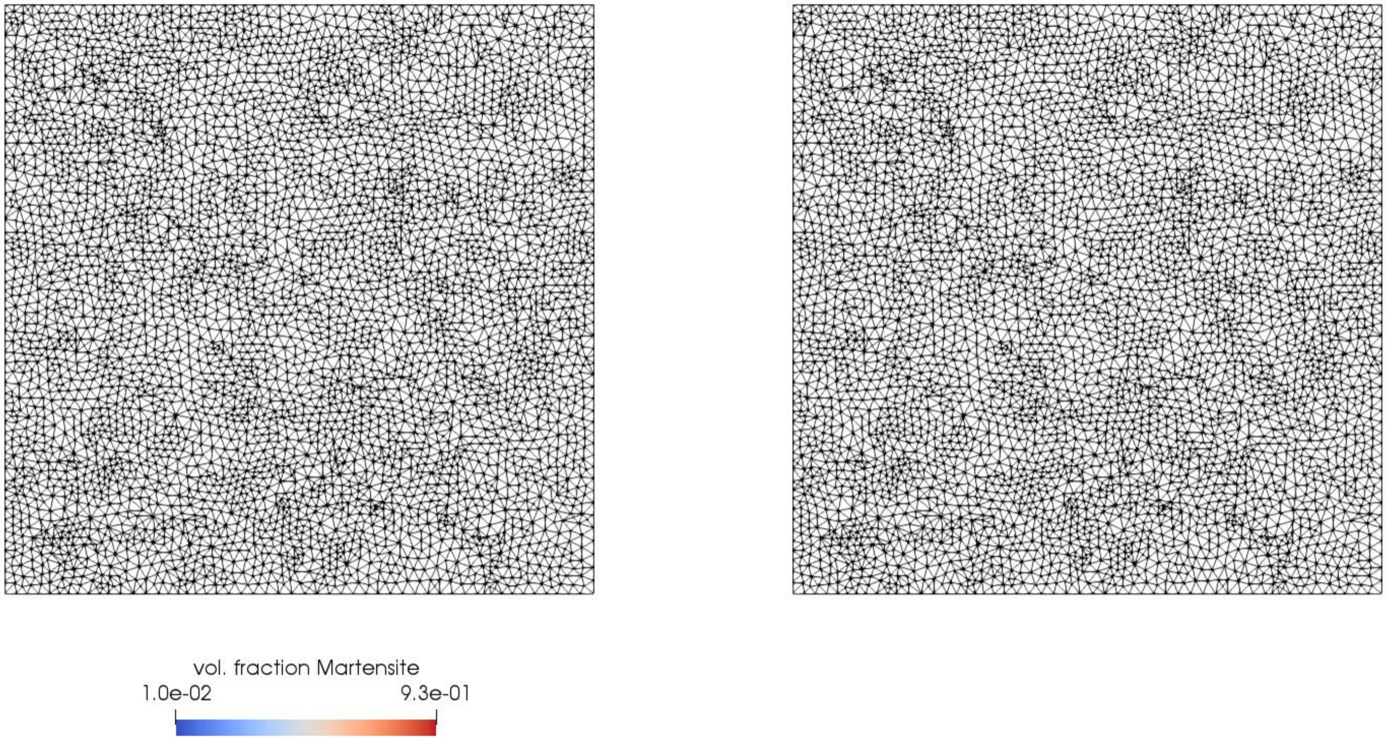

I. A. Rodrigues Lopes, et al (2023), *Eur. J. Mech. - A/Solids*, 102, 105104.

NUMERICAL EXAMPLE – STRAIN GRADIENTS AT CRACK TIP

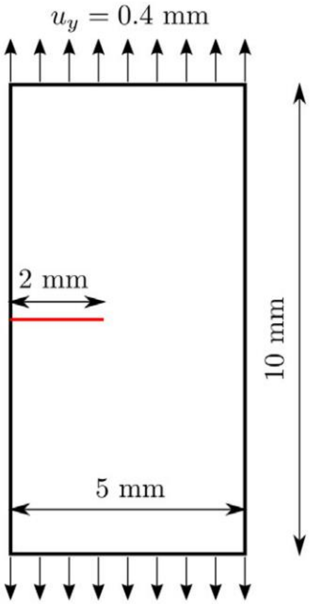

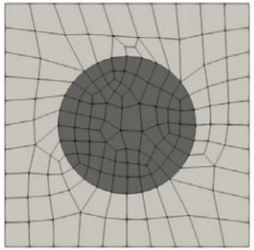

(b) Unit cell

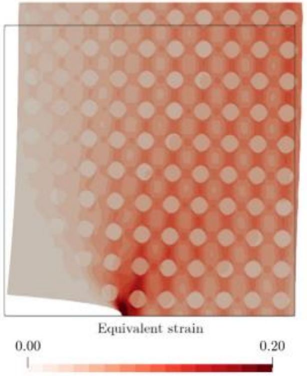

(a) DNS

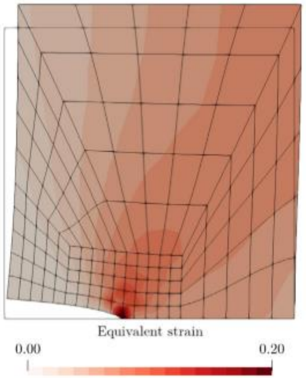

(c) Periodic

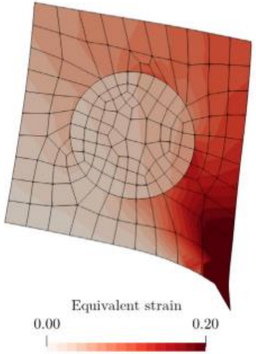

(a) DNS

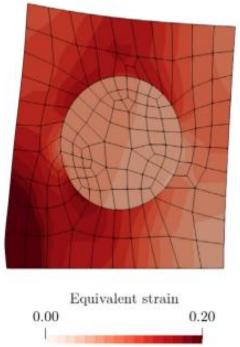

(a) DNS

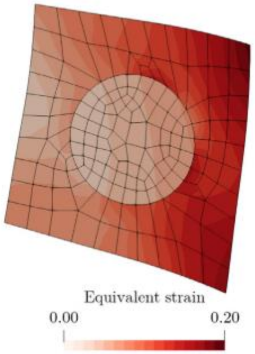

(c) Periodic

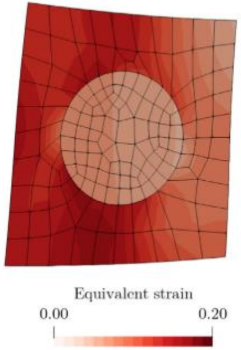

(c) Periodic

Rodrigues Lopes, I. A., & Andrade Pires, F. M. (2022).
Comput. Methods in Appl. Mech. Engrg, *392*, 114714.

SECOND-ORDER COMPUTATIONAL HOMOGENISATION

METAMATERIALS

W. F. dos Santos, I. A. Rodrigues Lopes, F. M. Andrade Pires, and S. P. B. Proença (2023), *Comput. Methods Appl. Mech. Eng.*, 416, 16374.

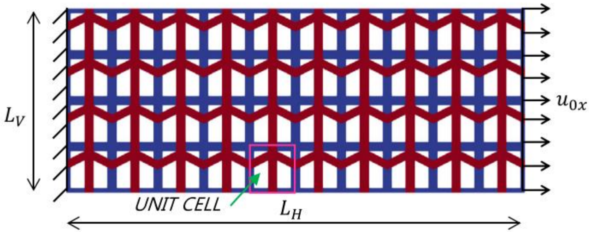

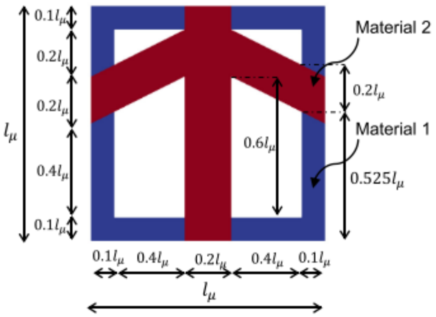

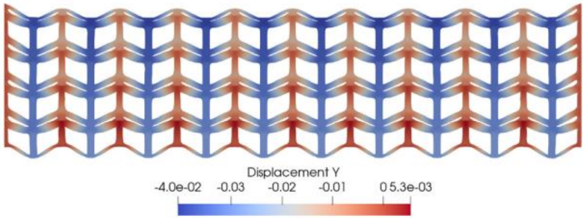

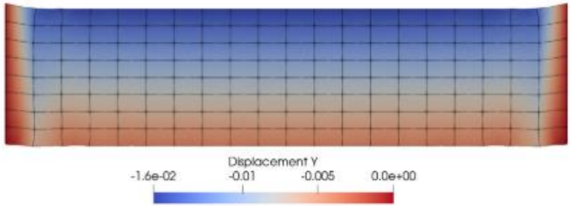

(c) Second-order: Periodic.

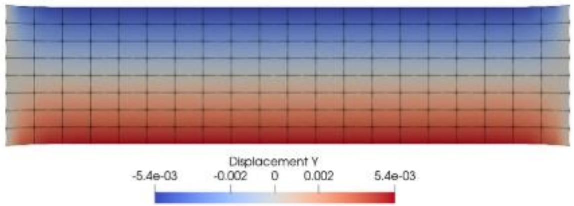

(d) First-order: Periodic.

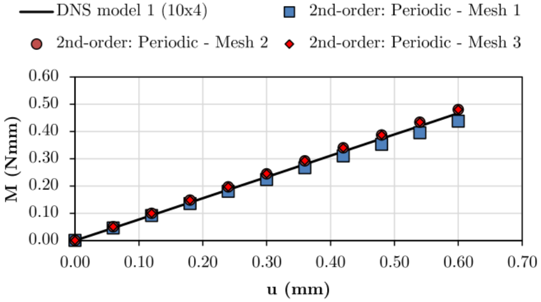

(c) Second-order: Periodic.

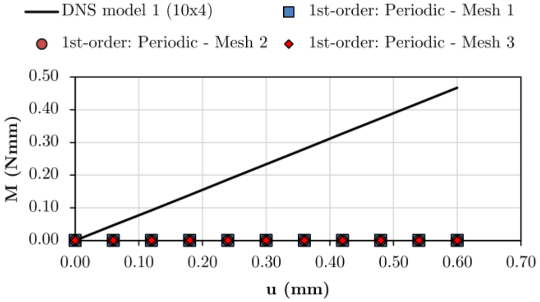

(d) First-order: Periodic.

SECOND-ORDER COMPUTATIONAL HOMOGENISATION

METAMATERIALS

W. F. dos Santos, I. A. Rodrigues Lopes, F. M. Andrade Pires, and S. P. B. Proença (2024), Int. J. Solids Struc.

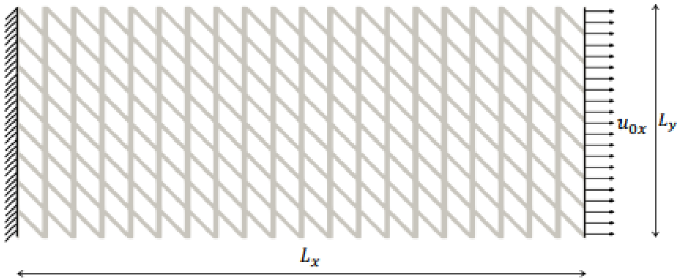

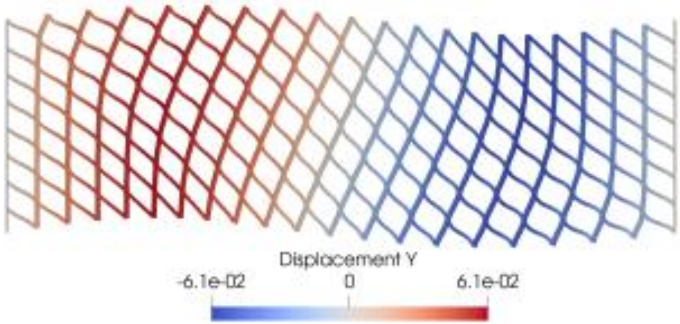

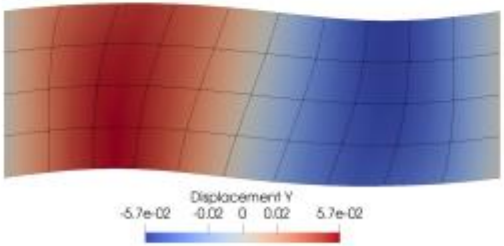

(b) Second-order: periodic.

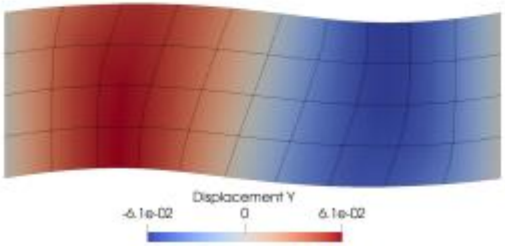

(e) First-order: periodic.

SECOND-ORDER COMPUTATIONAL HOMOGENISATION

METAMATERIALS

W. F. dos Santos, I. A. Rodrigues Lopes, F. M. Andrade Pires, and S. P. B. Proença (2024), Int. J. Solids Struc.

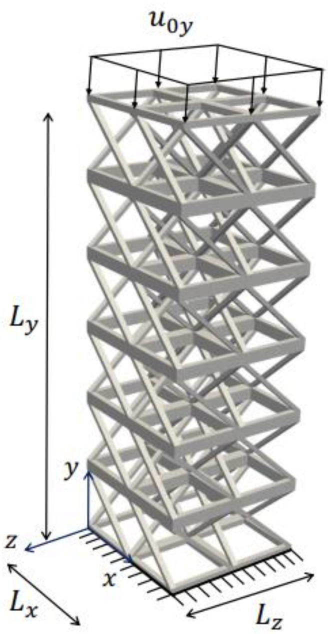

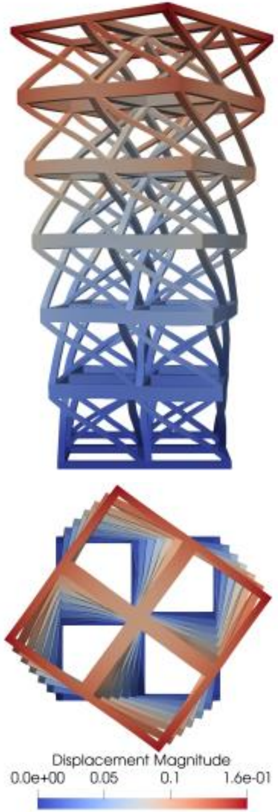

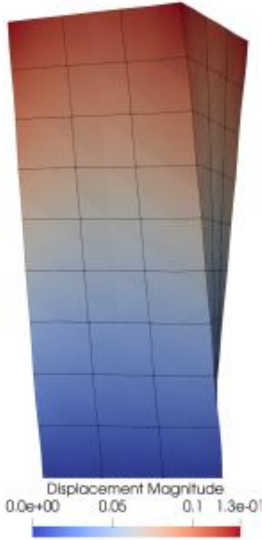

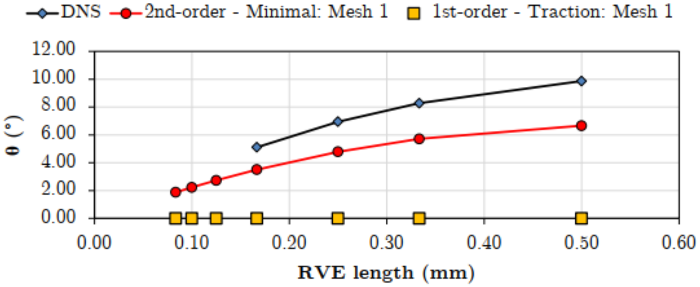

FULLY SECOND-ORDER COMPUTATIONAL HOMOGENISATION

CONCEPT

I. A. Rodrigues Lopes and F. M. Andrade Pires (2022), *Int. J. Numer. Methods Eng.*, 123(21), 5274–5318

Macro 2nd gradient continuum

$\boldsymbol{F}, \mathbf{G}$

Micro 2nd gradient continuum

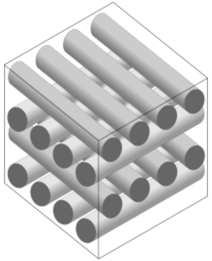

POSTULATED

Kinematic insertion

$$\boldsymbol{u}_\mu = (\boldsymbol{F} - \boldsymbol{I})\,\boldsymbol{Y} + \frac{1}{2}\mathbf{G} : (\boldsymbol{Y} \otimes \boldsymbol{Y}) + \tilde{\boldsymbol{u}}$$

$$\boxed{\hat{\boldsymbol{F}}_\mu = \boldsymbol{F} + \mathbf{G} \cdot \boldsymbol{Y} + \hat{\tilde{\boldsymbol{F}}}}$$

Kinematic homogenisation

$$\boldsymbol{F} = \frac{1}{V_\mu}\int_{\Omega_\mu} \boldsymbol{F}_\mu d\Omega_\mu$$

$$\boxed{\mathbf{G} = \frac{1}{V_\mu}\int_{\Omega_\mu} \mathbf{G}_\mu d\Omega_\mu}$$

Kinematic admissibility

1st Constraint: $\int_{\Omega_\mu} \nabla_Y \tilde{\boldsymbol{u}} dV = \boldsymbol{0} \Rightarrow \int_{\partial\Omega_\mu} \tilde{\boldsymbol{u}} \otimes \boldsymbol{N} dA = \boldsymbol{0}$

2nd Constraint: $\int_{\Omega_\mu} \tilde{\mathbf{G}}_\mu dV = \mathbf{0} \Rightarrow \int_{\Omega_\mu} \nabla^s_Y \hat{\tilde{\boldsymbol{F}}} dV = \boxed{\int_{\partial\Omega_\mu} \left(\hat{\tilde{\boldsymbol{F}}} \otimes \boldsymbol{N}\right)^S dA = \mathbf{0}}$

COMPATIBILITY

FULLY SECOND-ORDER COMPUTATIONAL HOMOGENISATION

ILLUSTRATION OF SIZE EFFECTS FROM THE MICRO-CONSTITUENTS

FE² boundary shear layer simulation

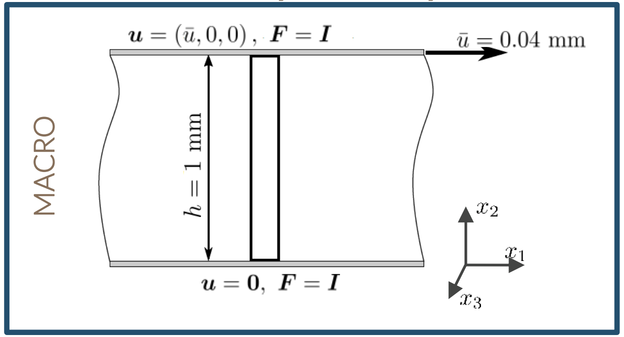

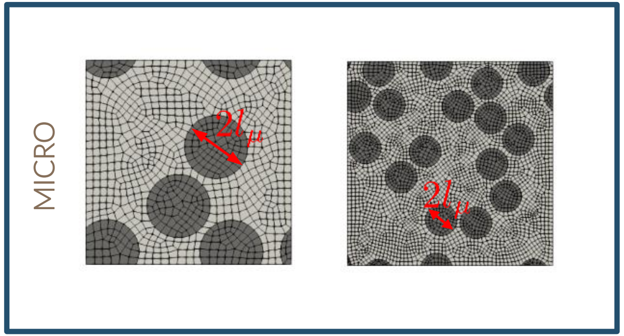

The **profile of deformation gradient** shear component is associated with the resulting **macroscopic length scale parameter**

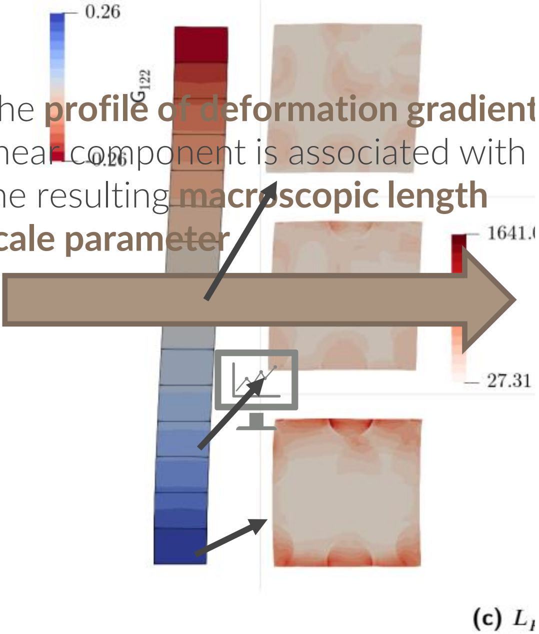

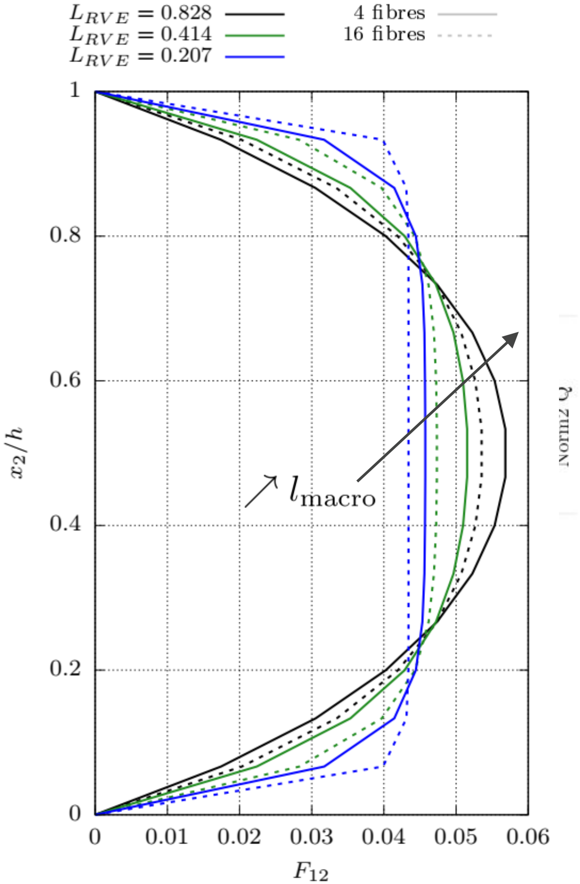

I. A. Rodrigues Lopes and F. M. Andrade Pires (2022), *Int. J. Numer. Methods Eng.*, 123(21), 5274–5318

FULLY SECOND-ORDER COMPUTATIONAL HOMOGENISATION

3D MIXED ELEMENTS AT BOTH SCALES

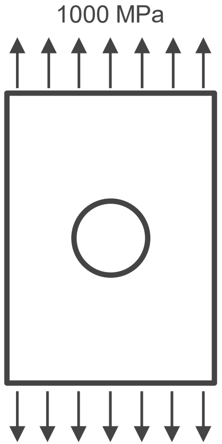

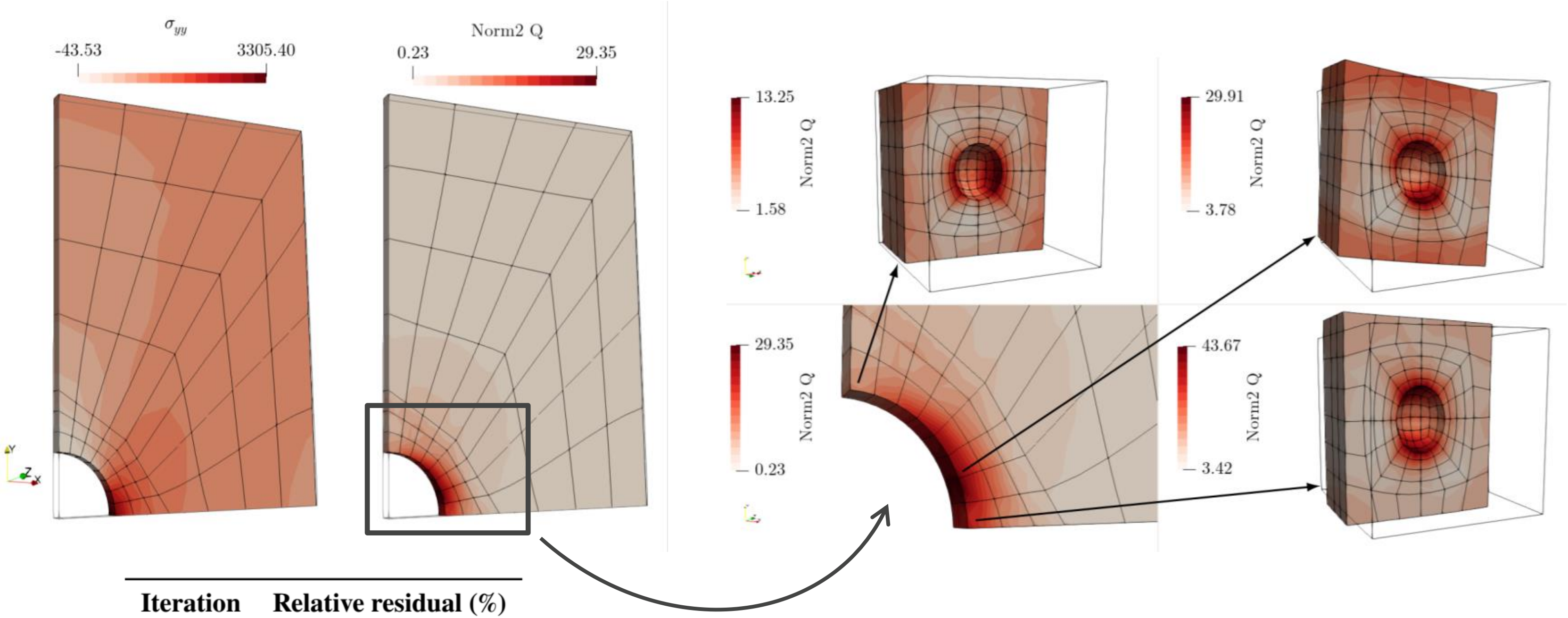

Iteration	Relative residual (%)
1	5.86
2	0.53×10^{-2}
3	0.21×10^{-6}

I. A. Rodrigues Lopes and F. M. Andrade Pires (2022), *Int. J. Numer. Methods Eng.*, 123(21), 5274–5318

COMPUTATIONAL HOMOGENISATION WITH FRACTURE

COMPUTATIONAL HOMOGENISATION WITH COHESIVE ELEMENTS

APPLICATION TO INTERGRANULAR FRACTURE

First-order computational homogenisation is enhanced with the presence of strong discontinuities

$$\boldsymbol{F} = \frac{1}{|\Omega_\mu|}\int_{\Omega_\mu} \boldsymbol{F}_\mu \, \mathrm{d}V + \frac{1}{|\Omega_\mu|}\int_{\Gamma_\mu} [\![\tilde{\boldsymbol{u}}_\mu]\!] \otimes \bar{\boldsymbol{n}}_\mu^{\Gamma} \, \mathrm{d}A.$$

An equivalent macroscopic crack is determined from the micro-cracks orientation

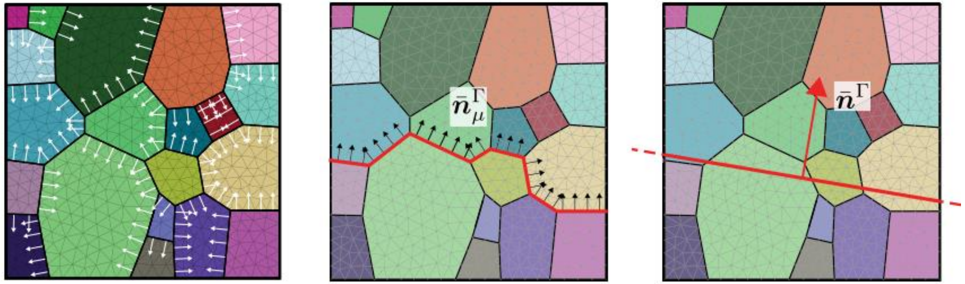

Macroscopic cohesive traction determined as the projection of the macro-stress on the macro-crack

$$\bar{\boldsymbol{t}} \equiv \boldsymbol{P}\,\bar{\boldsymbol{n}}^{\Gamma}$$

COMPUTATIONAL HOMOGENISATION WITH COHESIVE ELEMENTS

APPLICATION TO INTERGRANULAR FRACTURE

M. Vieira de Carvalho, I. A. Rodrigues Lopes, and F. M. Andrade Pires (2023), *Int. J. Plast.*, 71, 103780.

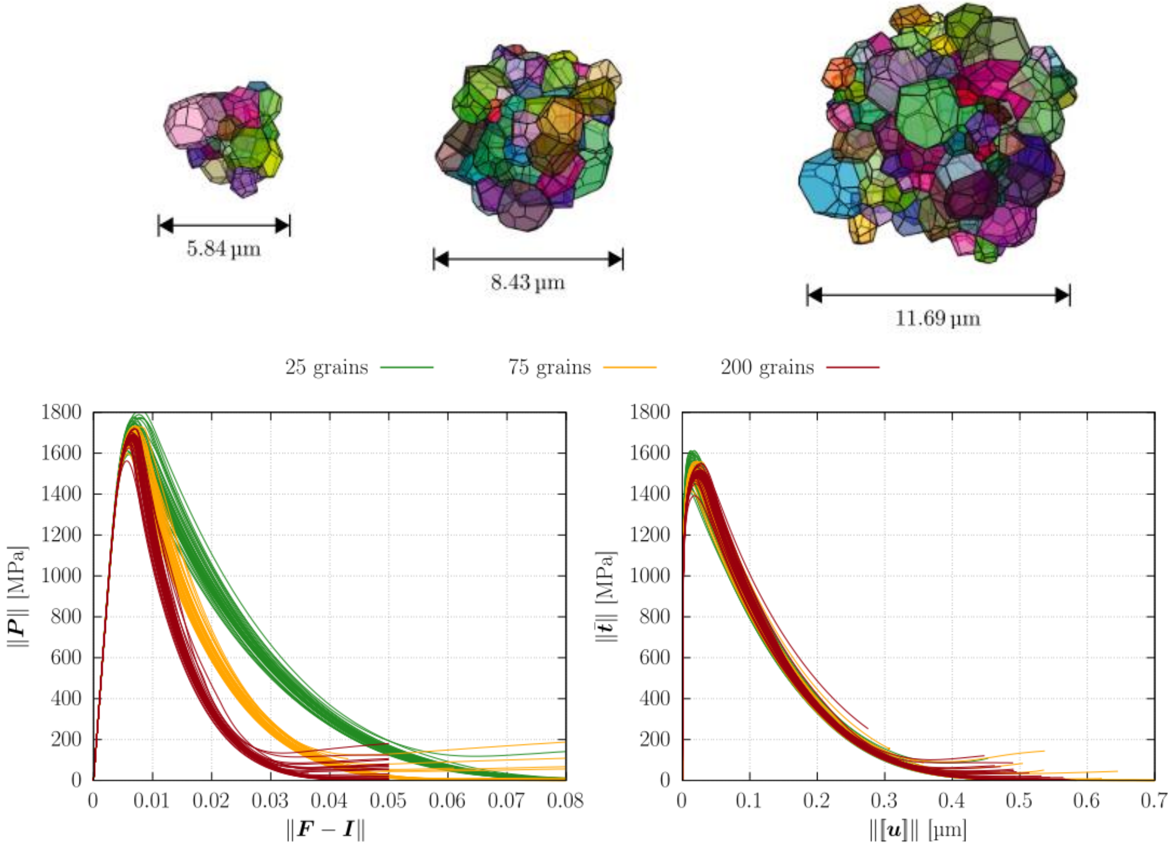

COMPUTATIONAL HOMOGENISATION WITH COHESIVE ELEMENTS

APPLICATION TO INTERGRANULAR FRACTURE

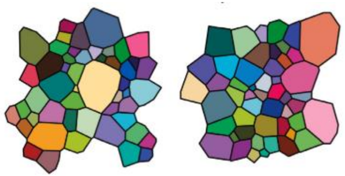

(a) Periodic tessellations.

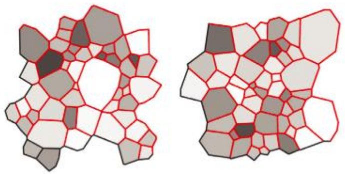

(c) Periodic cohesive elements.

(b) Non-periodic tessellations.

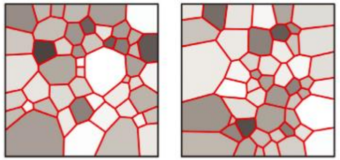

(d) Non-periodic cohesive elements.

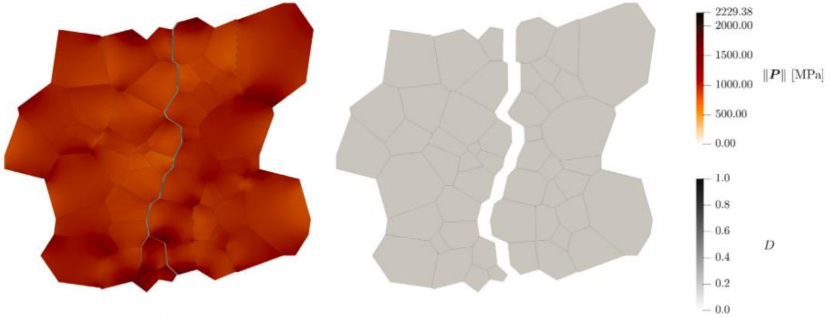

(a) $F_{xx} = 1.01$.

(b) $F_{xx} = 1.05$.

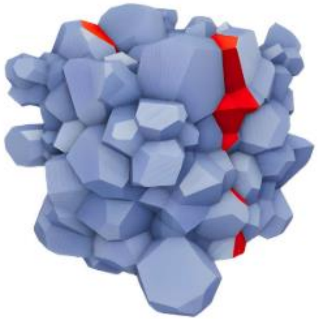

(a) Fracture surface.

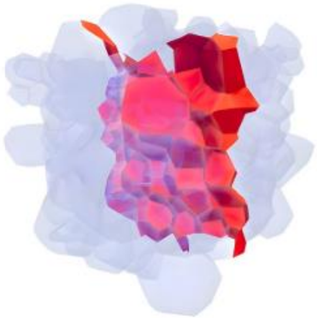

(b) Fracture surface highlighted.

MESO-SCALE MODELLING OF COMPOSITES

MODELLING COMPOSITES AT THE MESO-SCALE

CONCEPT

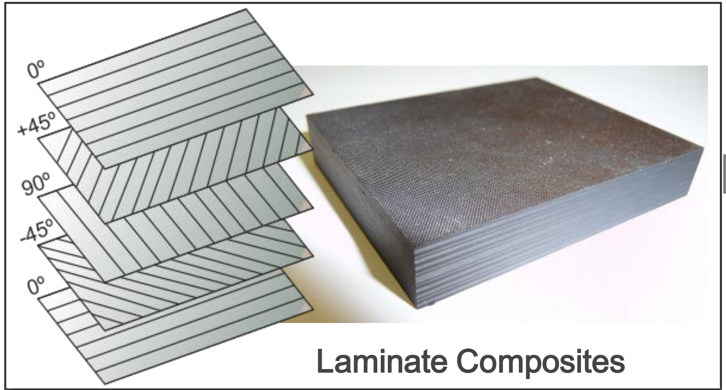

Laminate Composites

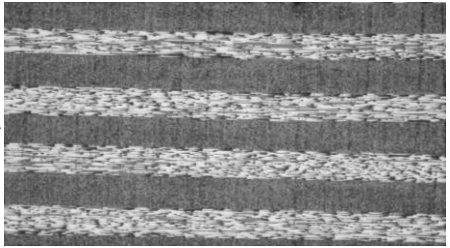

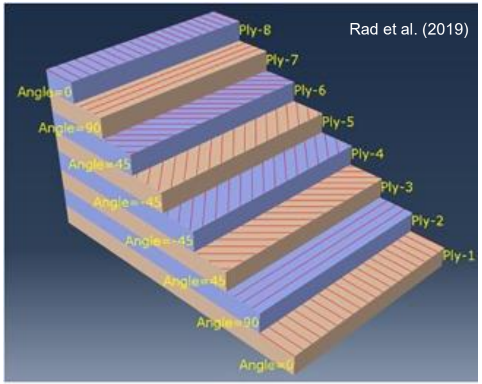

Meso-scale models
(at the ply level)

MODELLING COMPOSITES AT THE MESO-SCALE
REQUIREMENTS

What effects to be included in the models?

- **Transverse isotropy** (elastic and plastic domains)
- **Damage** Mechanisms
  - Matrix
  - Fibres
- **Visco-elasticity**
- **Visco-plasticity**
- **Finite strains**

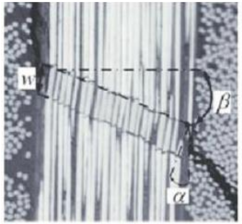

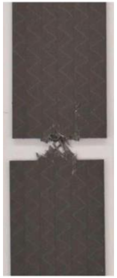

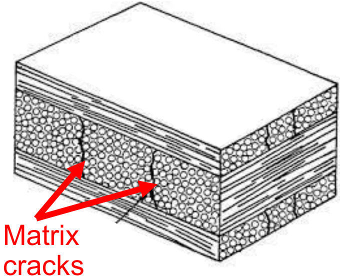

H. Koerber et al. / Mechanics of Materials 42 (2010) 1004–1019

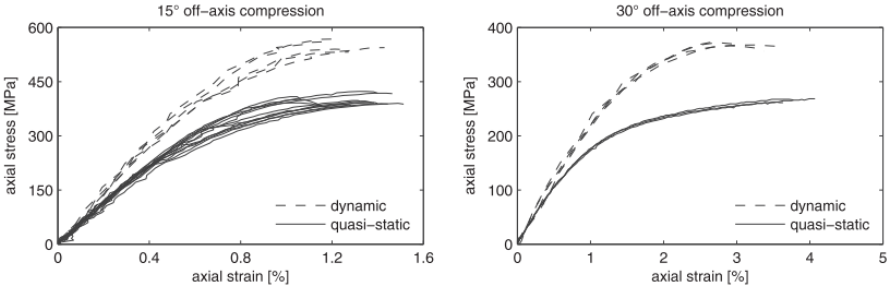

TRANSVERSE ISOTROPIC STRESS-STRAIN RELATIONSHIP AND VISCO-ELASTICITY

Elastic stress-strain relationship

$$\tilde{\boldsymbol{S}}_0 = \lambda \operatorname{tr}\left(\tilde{\boldsymbol{E}}^e\right)\boldsymbol{I} + 2\mu_T \tilde{\boldsymbol{E}}^e + \alpha\left[\operatorname{tr}\left(\tilde{\boldsymbol{A}}\tilde{\boldsymbol{E}}^e\right) + \operatorname{tr}\left(\tilde{\boldsymbol{E}}^e\right)\tilde{\boldsymbol{A}}\right]\boldsymbol{I}$$
$$+ 2\left(\mu_L - \mu_T\right)\left(\tilde{\boldsymbol{E}}^e\tilde{\boldsymbol{A}} + \tilde{\boldsymbol{A}}\tilde{\boldsymbol{E}}^e\right) + \beta \operatorname{tr}\left(\tilde{\boldsymbol{A}}\tilde{\boldsymbol{E}}^e\right)\tilde{\boldsymbol{A}}$$

Structural Tensor: $\tilde{\boldsymbol{A}} = \tilde{\boldsymbol{a}} \otimes \tilde{\boldsymbol{a}}$

Elastic Green-Lagrange: $\tilde{\boldsymbol{E}}^e = \frac{1}{2}\left(\tilde{\boldsymbol{C}}^e - \boldsymbol{I}\right)$

Elastic Parameters: $\begin{Bmatrix} \lambda \\ \alpha \\ \beta \\ \mu_T \\ \mu_L \end{Bmatrix} \leftrightarrow \begin{Bmatrix} E_{11} \\ E_{22} \\ G_{12} \\ \nu_{12} \\ \nu_{23} \end{Bmatrix}$

Rheological model: 1 Hooke element and 1 Maxwell element (Gerbaud et al., 2019)

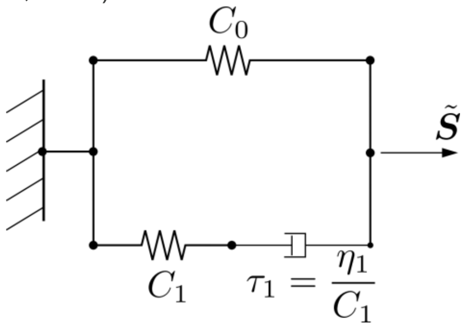

Finite strain theory of visco-elasticity (Kaliske, 2000)

$$\tilde{\boldsymbol{S}} = \tilde{\boldsymbol{S}}_0 + \tilde{\boldsymbol{S}}_1$$

$$\tilde{\boldsymbol{S}}_1^{n+1} = e^{-\frac{\Delta t}{\tau_1}}\tilde{\boldsymbol{S}}_1^n + \frac{1 - e^{-\frac{\Delta t}{\tau_1}}}{\frac{\Delta t}{\tau_1}}\gamma_1\left(\tilde{\boldsymbol{S}}_{0,n+1}^{\text{pind}} - \tilde{\boldsymbol{S}}_{0,n}^{\text{pind}}\right)$$

Rodrigues Lopes, et al. (2022). *International Journal of Solids and Structures*, 236, 111292.

3D INVARIANT-BASED VISCO-ELASTIC – VISCO-PLASTIC MODEL

TRANSVERSELY ISOTROPIC YIELD FUNCTION AND PLASTIC POTENTIAL

Yield function based on invariants

$$f\left(\tilde{\boldsymbol{\Sigma}}_s, \tilde{\boldsymbol{A}}, \bar{\varepsilon}^p\right) = \alpha_1 I_1 + \alpha_2 I_2 + \alpha_3 I_3 + \alpha_{32} I_3^2 - 1 \leq 0$$

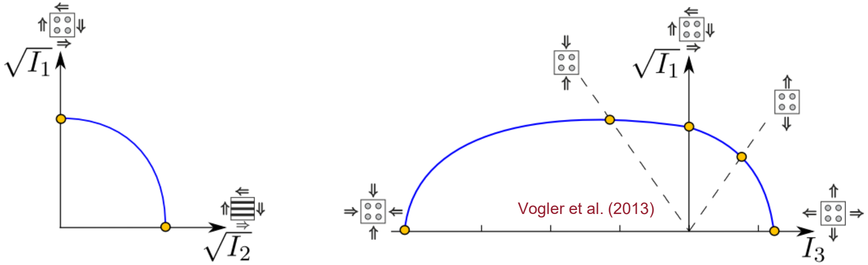

$$I_1 = \frac{1}{2}\left(\mathrm{tr}\,\tilde{\boldsymbol{\Sigma}}_s^{\mathrm{pind}}\right)^2 - \mathrm{tr}\left(\tilde{\boldsymbol{A}}\left[\tilde{\boldsymbol{\Sigma}}_s^{\mathrm{pind}}\right]^2\right),$$

$$I_2 = \mathrm{tr}\left(\tilde{\boldsymbol{A}}\left[\tilde{\boldsymbol{\Sigma}}_s^{\mathrm{pind}}\right]^2\right),$$

$$I_3 = \mathrm{tr}\,\tilde{\boldsymbol{\Sigma}}_s - \mathrm{tr}\left(\tilde{\boldsymbol{A}}\tilde{\boldsymbol{\Sigma}}_s\right)$$

Hardening parameters, α_i, determined from experimental curves obtained for different stress states

$$\alpha_1\left(\bar{\varepsilon}^p\right),\ \alpha_2\left(\bar{\varepsilon}^p\right),\ \alpha_3\left(\bar{\varepsilon}^p\right),\ \alpha_{32}\left(\bar{\varepsilon}^p\right),\ \dot{\bar{\varepsilon}}^p = \sqrt{\frac{1}{2}\tilde{\boldsymbol{D}}^p : \tilde{\boldsymbol{D}}^p}$$

Non-associative visco-plastic potential

$$g\left(\tilde{\boldsymbol{\Sigma}}_s, \tilde{\boldsymbol{A}}\right) = \beta_1 I_1 + \beta_2 I_2 + \beta_{32} I_3^2 - 1 = \frac{1}{2}\tilde{\boldsymbol{\Sigma}}_s : \mathbb{M} : \tilde{\boldsymbol{\Sigma}}_s$$

Parameters (β_i) calibrated to obtained a given plastic Poisson's ratio (Vogler et al., 2013)

Flow tensor and rate of plastic deformation:

$$\boldsymbol{N}_g = \frac{\partial g\left(\tilde{\boldsymbol{\Sigma}}_s, \tilde{\boldsymbol{A}}\right)}{\partial \tilde{\boldsymbol{\Sigma}}_s} = \mathbb{M} : \tilde{\boldsymbol{\Sigma}}_s.$$

$$\tilde{\boldsymbol{D}}^p = \dot{\gamma}\boldsymbol{N}_g$$

Perzyna model employed to describe the evolution of the plastic multiplier rate

$$\dot{\gamma} = \frac{\left\langle f^m\left(\tilde{\boldsymbol{\Sigma}}_s, \tilde{\boldsymbol{A}}, \bar{\varepsilon}^p\right)\right\rangle}{\eta}$$

Rodrigues Lopes, et al. (2022). *International Journal of Solids and Structures*, 236, 111292.

3D INVARIANT-BASED VISCO-ELASTIC – VISCO-PLASTIC MODEL
NNUMERICAL EXAMPLES – OFF-AXIS COMPRESSION

HexPly IM7-8552 (carbon fibre in epoxy matrix)
Constitutive parameters calibrated by
[Vogler et al., 2013; Koerber, et al., 2018, Gerbaud et al. 2019]

Quasi-static tests ($10^{-4}\ s^{-1}$) and dynamic tests ($100\ s^{-1}$)
[Koerber, et al., 2010].

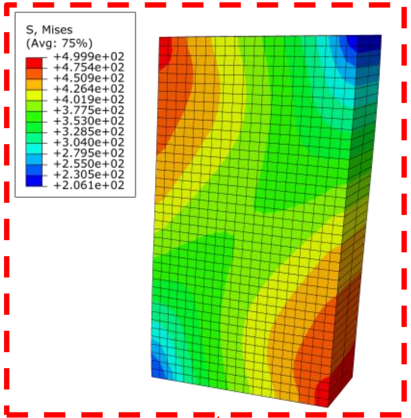

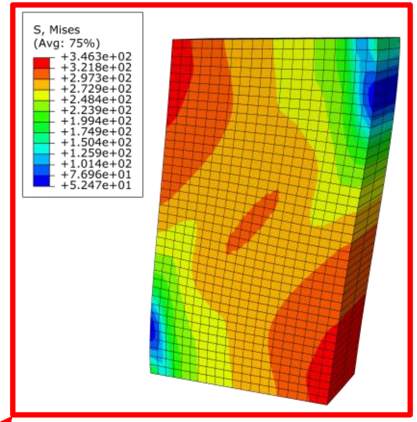

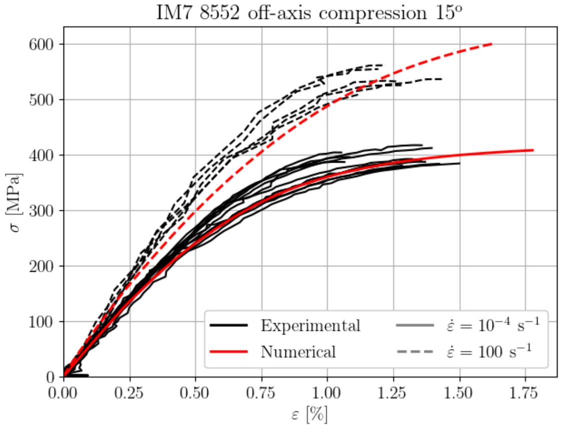

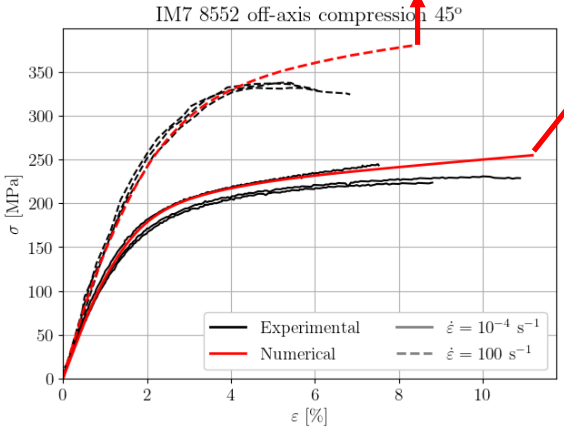

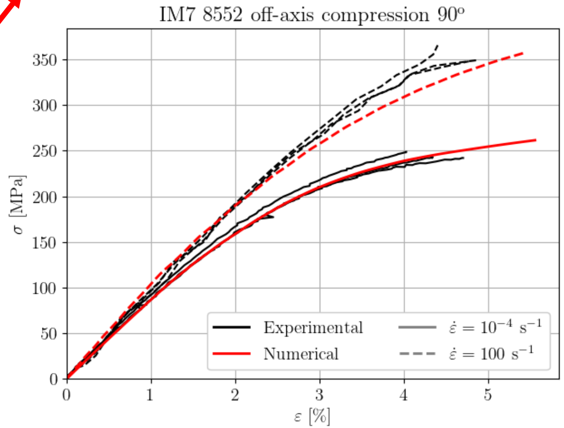

Rodrigues Lopes, et al. (2022). *International Journal of Solids and Structures*, 236, 111292.

FINITE STRAIN SMEARED-CRACK MODEL

CONCEPT

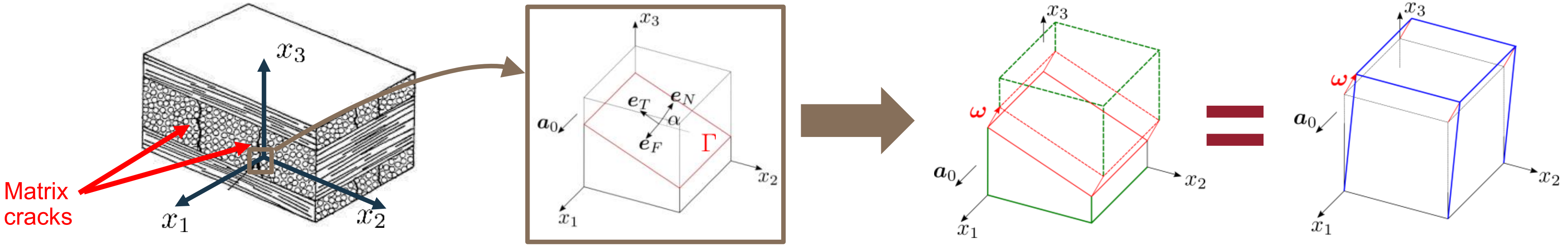

Transverse failure criterion [Camanho et al., 2015]

$$f_T(\boldsymbol{\sigma}, \boldsymbol{A}) = \zeta_1 \bar{I}_1 + \zeta_2 \bar{I}_2 + \zeta_3 \bar{I}_3 + \zeta_{32} \bar{I}_3^2 - 1 \leq 0$$

Additive Deformation Gradient Decomposition [Leone, 2015]

$$\boxed{\boldsymbol{F}_B} + \boxed{\nabla \boldsymbol{u}_c} = \boxed{\boldsymbol{F}}$$

Based on **homogenisation considerations**...

$$\boldsymbol{F}_B = \boldsymbol{F} - \boxed{\frac{|\Gamma|}{V_B} \boldsymbol{R}_\alpha \boldsymbol{\omega} \otimes \boldsymbol{e}_N}$$

Non-linear equilibrium between bulk stress and cohesive tractions:

$$\boldsymbol{P}(\boldsymbol{F}_B) \cdot \boldsymbol{e}_N = \boldsymbol{R}_\alpha \cdot \boldsymbol{\tau}(\omega)$$

Cohesive law – defines cohesive tractions on the crack

normal

$$\begin{cases} \tau_N = (1-d)\,|\bar{\tau}_N|\,, & \text{if } \omega_N \geq \omega_N^{max} \\ \tau_N = (1-d)\,|\bar{\tau}_N|\,\dfrac{\omega_N}{\omega_N^{max}}, & \text{if } 0 \leq \omega_N < \omega_N^{max} \\ \tau_N = k_N \omega_N, & \text{if } \omega_N \leq 0 \end{cases}$$

shear

$$\begin{cases} \tau_s = (1-d)\,\bar{\tau}_s, & \text{if } \omega_s \geq \omega_s^{max} \\ \tau_s = (1-d)\,\bar{\tau}_s \dfrac{\omega_s}{\omega_s^{max}}, & \text{if } \omega_s < \omega_s^{max} \end{cases}$$

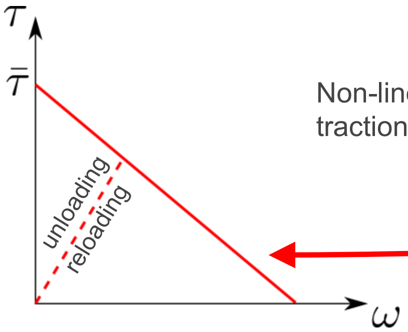

Rodrigues Lopes, et al. (2023). *International Journal of Solids and Structures*, 282, 112449.

LONGITUDINAL FAILURE
A CONTINUUM DAMAGE APPROACH

Longitudinal failure criterion

$$f_L = \phi_L - r_L \leq 0$$

$$\phi_L = \begin{cases} \dfrac{E_1}{X_T} E_{B,11}, & \text{if } E_{B,11} \geq 0 \\ \dfrac{E_1}{X_C} E_{B,11}, & \text{if } E_{B,11} < 0 \end{cases}$$

$$r_L = \max\left(1, \max\left(\phi_L\right)\right)$$

Damaged stress-strain relationship [Maimì, 2007]

$$\mathbf{E}_B = \mathbf{HS} \Leftrightarrow \mathbf{S} = \mathbf{H}^{-1}\mathbf{E}_B$$

$$\mathbf{H} = \begin{bmatrix} \dfrac{1}{E_{11}(1-d_1)} & -\dfrac{\nu_{21}}{E_{22}} & -\dfrac{\nu_{21}}{E_{22}} & 0 & 0 & 0 \\ & \dfrac{1}{E_{22}} & -\dfrac{\nu_{23}}{E_{22}} & 0 & 0 & 0 \\ & & \dfrac{1}{E_{22}} & 0 & 0 & 0 \\ & & & \dfrac{1}{G_{12}} & 0 & 0 \\ & \text{sym} & & & \dfrac{1}{G_{23}} & 0 \\ & & & & & \dfrac{1}{G_{12}} \end{bmatrix}$$

Evolution of the damage variable
Crack band model [Bažant, 1983]

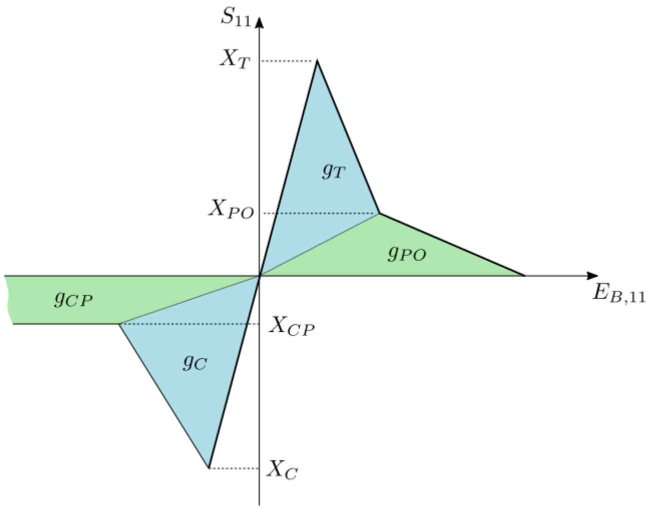

Rodrigues Lopes, et al. (2023). *International Journal of Solids and Structures*, 282, 112449.

FINITE STRAIN SMEARED-CRACK MODEL
NUMERICAL RESULTS – QI-OPEN-HOLE

Quasi-isotropic $[90/0/+-45]_{3S}$ open-hole tension
HexPly IM7-8552

Numerical Curves

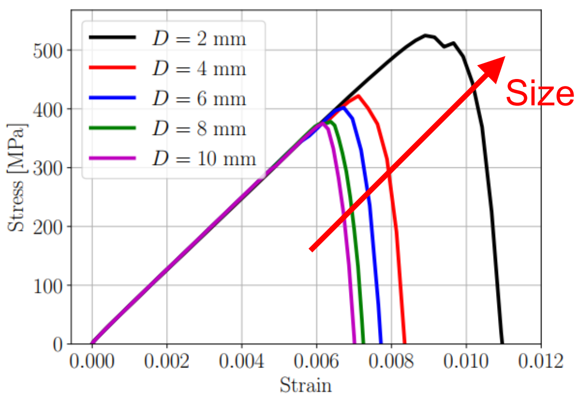

Strength comparison with experimental data (Camanho et al., 2007)

Hole diameter (mm)	Strength (MPa)		
	Experimental	Numerical	
2	555.7	524.7	-5.6%
4	480.6	422.1	-12.2%
6	438.7	402.1	-8.3%
8	375.7	378.2	0.7%
10	373.7	375.3	0.4%

Transverse damage

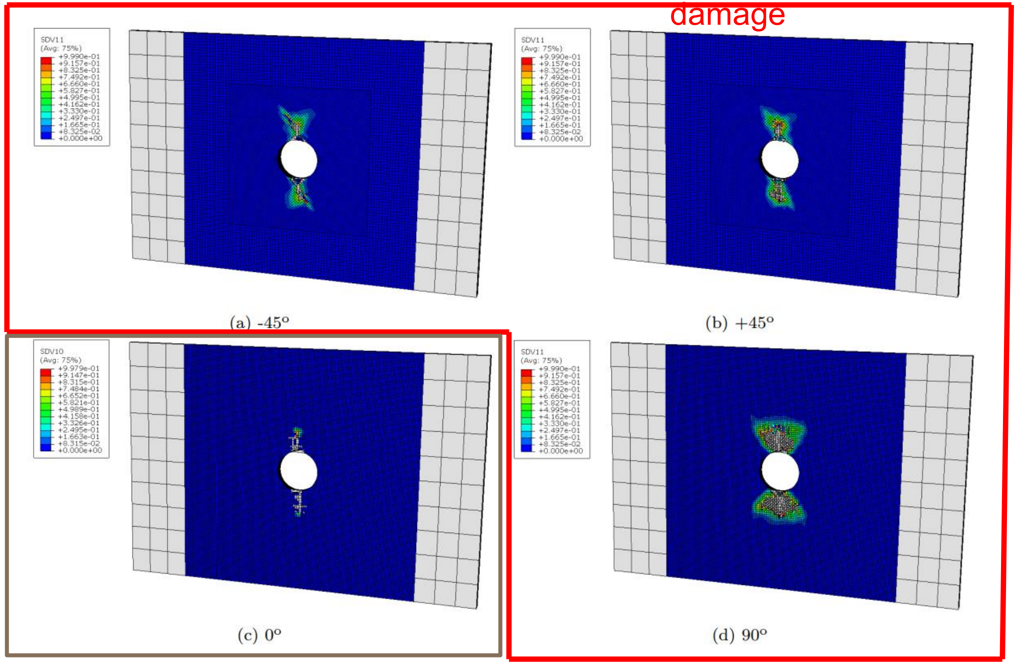

Longitudinal damage

Rodrigues Lopes, et al. (2023). *International Journal of Solids and Structures*, 282, 112449.

FINITE STRAIN SMEARED-CRACK MODEL
COUPLING WITH VISCO-ELASTIC – VISCO-PLASTIC MODEL

Longitudinal Shear

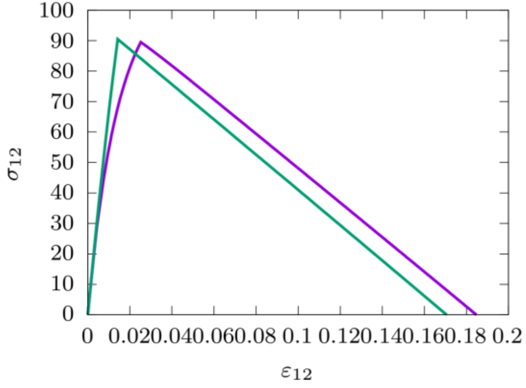

Transverse Tension

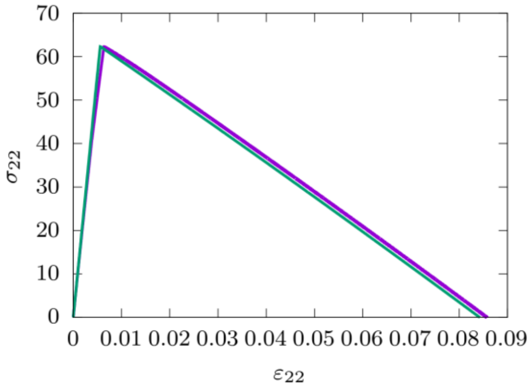

Transverse Compression

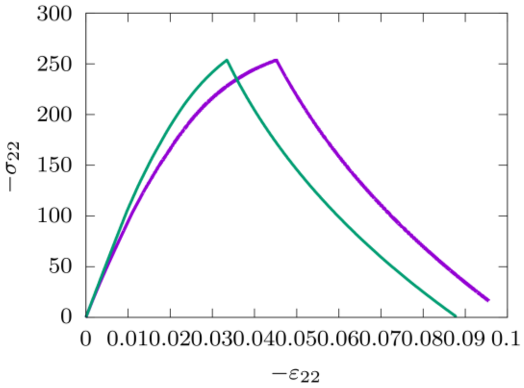

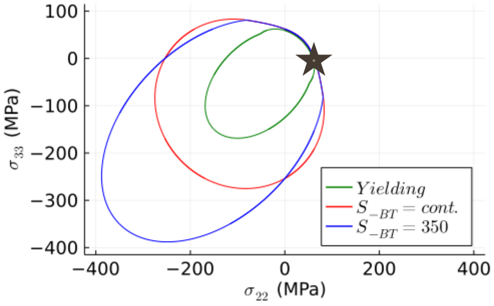

ACKNOWLEDGEMENTS

ACKNOWLEDGEMENTS

- BSC/Severo Ochoa Mobility Program – Incoming Grant
- Clean Sky 2 Joint Undertaking (JU) – **TREAL** project — Thermoplastic material allowable generation using a reliability-based virtual modeling platform (Grant agreement No. 864723)
- European Union’s Horizon 2020 research and innovation programme – **DIDEAROT** project – Digital strategies for robust manufacturing and design of composite aircraft (Grant agreement No. 101056682)
- Fundação para a Ciência e a Tecnologia – PhD Grant: SFRH/BD/100093/2014

driving science & innovation

CONVERTING KNOWLEDGE INTO VALUE FOR OVER 35 YEARS

Since 1986

Multi-scale Modelling of Complex Materials undergoing Strain Gradients and Damage

Severo Ochoa Seminar

Igor A. Rodrigues Lopes
ilopes@inegi.up.pt

INSTITUTE OF SCIENCE AND INNOVATION IN MECHANICAL AND INDUSTRIAL ENGINEERING

www.inegi.pt

BSC-CNS, Barcelona, 21 February 2024